AD-A119 945 SCIENCE APPLICATIONS INC LA JOLLA CA F/G 18/8
RADIATION FIELD CHARACTERIZATION FOR THE AFRRI TRIGA REACTOR. V--ETC(U)
JUN 81 V V VERBINSKI, K FERLIC DNA001-80-C-0308
UNCLASSIFIED SAI-272-A1-183RI-LJ DNA-5793F-1 NL

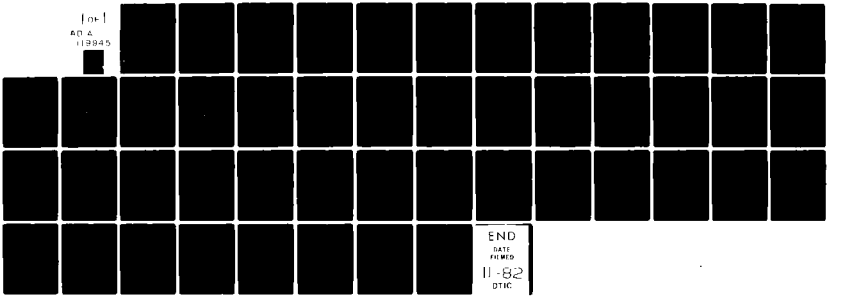

(12)

DNA 5793F-1

RADIATION FIELD CHARACTERIZATION FOR THE AFRRI TRIGA REACTOR

Volume I-Baseline Measurements and Evaluation of Calculational Data

Science Applications, Incorporated
P. O. Box 2351
La Jolla, California 92038

1 June 1981

Final Report for Period 5 May 1980—31 December 1980

CONTRACT No. DNA 001-80-C-0308

APPROVED FOR PUBLIC RELEASE;
DISTRIBUTION UNLIMITED.

THIS WORK SPONSORED BY THE DEFENSE NUCLEAR AGENCY
UNDER RDT&E RMSS CODE B350080464 U99QAXMJ00068 H2590D.

Prepared for
Director
DEFENSE NUCLEAR AGENCY
Washington, D. C. 20305

UNCLASSIFIED

SECURITY CLASSIFICATION OF THIS PAGE (When Data Entered)

REPORT DOCUMENTATION PAGE

READ INSTRUCTIONS BEFORE COMPLETING FORM

1. REPORT NUMBER: DNA 5793F-1	2. GOVT ACCESSION NO.: AD-A119745
3. RECIPIENT'S CATALOG NUMBER:	
4. TITLE (and Subtitle): RADIATION FIELD CHARACTERIZATION FOR THE AFRRI TRIGA REACTOR, Volume I—Baseline Measurements and Evaluation of Calculational Data	5. TYPE OF REPORT & PERIOD COVERED: Final Report for Period 5 May 80—31 Dec 80
	6. PERFORMING ORG. REPORT NUMBER: SAI-272-81-183RI-LJ
7. AUTHOR(s): Victor V. Verbinski/SAI, Costa C. Cassapakis/SAI, William K. Hagan/SAI, Lt. Ken Ferlic/AFRRI, Capt. Eric Daxon/AFRRI	8. CONTRACT OR GRANT NUMBER(s): DNA 001-80-C-0308
9. PERFORMING ORGANIZATION NAME AND ADDRESS: Science Applications, Incorporated, P.O. Box 2351, La Jolla, California 92038	10. PROGRAM ELEMENT, PROJECT, TASK AREA & WORK UNIT NUMBERS: Subtask U99QAXNJ000-63
11. CONTROLLING OFFICE NAME AND ADDRESS: Director, Defense Nuclear Agency, Washington, D.C. 20305	12. REPORT DATE: 1 June 1981
	13. NUMBER OF PAGES: 50
14. MONITORING AGENCY NAME & ADDRESS (if different from Controlling Office)	15. SECURITY CLASS. (of this report): Unclassified
	15a. DECLASSIFICATION/DOWNGRADING SCHEDULE: N/A Since UNCLASSIFIED

16. DISTRIBUTION STATEMENT (of this Report)

Approved for public release; distribution unlimited

17. DISTRIBUTION STATEMENT (of the abstract entered in Block 20, if different from Report)

18. SUPPLEMENTARY NOTES

This work sponsored by the Defense Nuclear Agency under RDT&E RMSS Code B350080464 U99QAXNJ00068 H2590D.

19. KEY WORDS (Continue on reverse side if necessary and identify by block number)

Radiation
Neutron-Spectral Measurements
Gamma-Ray
Reactor
AFRRI TRIGA

20. ABSTRACT (Continue on reverse side if necessary and identify by block number)

This document summarizes the neutron spectral measurements and the neutron and gamma-ray spectral calculations for five different irradiation geometries commonly employed in biological and semiconductor radiation-damage studies: freefield in both ER1 and ER2 exposure rooms; behind a 2-inch lead wall and inside an exercise wheel; behind a 6-inch lead wall and inside a 2-inch lead cave; and at the center of a tissue-equivalent phantom located behind a 6-inch lead wall.

DD FORM 1 JAN 73 1473 EDITION OF 1 NOV 65 IS OBSOLETE

UNCLASSIFIED

SECURITY CLASSIFICATION OF THIS PAGE (When Data Entered)

TABLE OF CONTENTS

LIST OF ILLUSTRATIONS

LIST OF TABLES

1. INTRODUCTION

1.1 Rationale for the Measurements/Calculations

This document summarizes the neutron spectral measurements and the neutron and gamma-ray spectral calculations for five different irradiation geometries commonly employed in biological and semiconductor radiation-damage studies: free field in both ER1 and ER2 exposure rooms; behind a 2-inch lead wall and inside an exercise wheel; behind a 6-inch lead wall and inside a 2-inch lead cave; and at the center of a tissue-equivalent phantom located behind a 6-inch lead wall. Not only does the gamma to neutron dose ratio change considerably from one of these configurations to the next, but the neutron spectrum changes very significantly for each perturbation of the free-field measurement. (In fact, the free-field spectrum itself changes measurably with distance from the reactor[1], because of the relatively greater effect of room-scattered neutrons with increasing distance (R) from the center of the reactor: The fast neutrons from the reactor fall-off approximately as $1/R^2$ while the room-scattered component is more nearly constant with R, the distance from the reactor core center.) The methods of "hardening" or "softening" the fast neutron spectrum are presented in Section 4.

Accurate neutron spectral measurements were made for the five different configurations. The neutron-transport calculations were carried out for the same cases with geometric approximations that varied from a spherical geometry (of various "shells" of reactor core, aluminum, air, lead, water, and the distant walls) to a 3-dimensional (3-D) model of the actual geometry. The measurements utilized the calculated spectrum shape in each case as a starting (trial) spectrum, and the final unfolded spectrum was obtained with only a few small shape-varying iterations. This only occurs when the calculated spectrum and the measured are in good agreement, and verifies the accuracy of the calculated spectral shape.

Once the accuracy of the calculated spectral shapes have been verified with multiple-foil measurements, the magnitude is obtained with the use of a single multiplying factor (normalization constant). This normalization factor is required to correct for uncertainties in the absolute neutron output of the reactor per power-monitor count (power calibration), in power distribution throughout the reactor, and the (variable) water thickness layer between the reactor core and the exposure-room aluminum "window". Some smaller uncertainties can arise from cross-section approximations and finite energy group widths but these and the previously mentioned uncertainties are completely resolved by renormalization of the calculation (by determining the simple "correction constant") to the nearest configuration measured.

With the baseline measurements/calculations presented here, one can very accurately calculate the biological dose and thus calibrate all the fast neutron dosimetry devices used with the AFRRI reactor, inluding the sulfur or nickel neutron flux monitor. All of the above applies to fast neutron flux.

For thermal neutrons, a cadmium-difference measurement with manganese or (very thin) gold foils or other thermal-neutron sensitive device is adequate. The measurement of the thermal neutron flux is an absolute, single-point measurement. On the other hand, the accurate calculation of thermal-neutron flux is subject to variations due to small material and geometric uncertainties, including the amount of neutron-absorbing impurities in the room structure and that of the added shields/moderators which is generally very poorly known. Thus, a careful measurement is much preferred.

Returning to the fast neutron flux, it should be pointed out that once the spectral shape has been accurately determined by a calculation such as the ones experimentally verified here, only one threshold foil dosimeter is subsequently needed to fix the absolute magnitude: Thus the power of the calculations for future use such as in the design of biological/material exposure is clear.

The gamma-ray dose variability can be ascertained with adequate accuracy using a number of well characterized dosimeters. The RBE (relative biological effectiveness) does not depart much from unity for gamma-rays, unlike neutrons for which the RBE varies by about a factor of 10 between slow and fast neutrons. The neutron damage to electronic devices varies by even a greater factor[2]. Thus, for the AFRRI reactor exposures, the characterization of the radiation field in the work presented below is concerned chiefly with determinations of the neutron spectral flux.

The calculations of gamma-ray spectra (presented in Volume II of this report) are obtained by using coupled neutron and gamma-ray cross sections. The gamma-ray field is mostly made up of direct gamma-rays from the reactor core, inelastic scattering of fast neutrons, and thermal-neutron-capture gamma-rays. Because of the uncertainty in thermal neutron flux, the calculation of the capture gamma-ray flux is not expected to be nearly as accurate as the calculation of the fast neutron flux: This is important behind lead shields where a large fraction of the total gamma-ray dose may be due to capture-neutron gamma-rays.

1.2 Past Work

The spectral characteristics of the neutron field were measured almost two decades ago by W. Quam of E.G.&G. and first reported in October, 1964. A later summary appeared in a compilation by J.A. Sayeg[3]. In this work, the gross spectral dependence of the neutron field was measured with the use of three threshold foils, and also with some foils without an energy threshold (E_{th}) but with boron and cadmium shields to produce effective (mechanical) low energy thresholds of about 0.01 MeV and 4×10^{-7} MeV, respectively. The foils and their threshold energies were $^{32}S(E_{th} \simeq 3$ MeV), $^{238}U(E_{th} \simeq 1.5$ MeV), $^{237}Np(E_{th} \simeq 0.5$ MeV), $^{239}Pu(E_{th} \simeq 0.01$ MeV via boron shield), and $^{197}Au(E_{th} \simeq$ 0.01 MeV, 4×10^{-7} MeV, and 0 MeV via boron shield, cadmium shield, and unshielded foils respectively.)

For the fission foils, gross fission-product gamma-ray counting was done, with essentially all the gamma rays being counted. The count rate versus irradiation time, wait time, and count time was calibrated with a very complex

procedure which leaves much to be desired in terms of accuracy. Furthermore, the non-fission-product radioactivity must be somehow estimated and subtracted in this type of measurement. This adds significantly to the uncertainties of these early measurements, especially for fission foils such as ^{237}Np which are highly radioactive before being exposed to the neutron field being measured.

1.3 Present Work

The state of the art has advanced considerably since the early 1960's in neutron spectrum measurements in terms of radioactivity-counting techniques; nuclear decay schemes/fluorescent yields/fission-product yields; cross section data; large-computer-based spectrum-unfolding codes; and neutron transport calculations to provide a good trial spectrum for the neutron-spectrum unfolding code. These advancements are presented in recent ASTM Procedures[4], which were essentially derived from the work presented in Reference 5. The work presented here was carried out by the same methods and, in fact, by the same investigators. Some recent improvements have been added. These involve some more accurate nuclear data on the threshold-foil cross sections and gamma-ray fields, and more careful measurements of thermal and near-epithermal neutron spectral data (which were of little interest to radiation damage characterization to silicon semiconductor devices addressed in the ASTM Standard Procedures[4]).

2. FIELD CHARACTERIZATION MEASUREMENTS

2.1 Foil Measurement Methods

Five baseline spectral measurements were performed corresponding to the most frequently utilized irradiation configurations. The characteristics of these five reactor runs are shown in Table 1 and the experimental configuration for each is shown in Figures 1 through 5. The characteristics of the seventeen threshold foils used to measure the above neutron spectra are shown in Table 2.

Three threshold foil sets were used for each spectral measurement. The first was a complete set of all seventeen foils and was enclosed in a 1.65 g/cm^2 boron sphere; the second set contained one ^{197}Au, one ^{55}Mn and three ^{58}Ni foils, all enclosed in a 0.020 inch (.050 cm) thick cadmium cover, and the third set contained one ^{197}Au, one ^{55}Mn and three ^{58}Ni foils, with all five foils in "bare" (no cover) configuration.

The use of the ^{10}B sphere is important for two reasons. First, it provides an effective threshold of about 0.01 MeV for the ^{197}Au, the ^{55}Mn, and ^{235}U foils; and second, it reduces drastically the effects of isotopic impurities in the foils that lead to the same product nucleus as the reactions of interest via the much more efficient route of thermal neutron activation. For instance, the reactions Al(n, α) and ^{23}Na(n, γ) lead to the same product nucleus, but the second one is activated by thermal neutrons that have a very large reaction cross section. Thus, in this case, sodium contamination of the aluminum foils (surface contamination, say) must be kept very small.

The use of the cadmium-covered and "bare" foils provides an excellent method for determining the thermal neutron flux by first determining the total flux from the "bare" foils and then subtracting out the epithermal flux determined from the cadmium-covered foils.

Finally, the ^{58}Ni foils in the "bare" foil set are used in conjunction with the ^{58}Ni foils in the ^{10}B sphere to provide a correction factor for the ^{10}B shielding effect on the foils with $E_{th} \gtrsim 1$ MeV. These ^{58}Ni foils are used with ^{32}S foils at some dosimetry laboratories because they are inherently more accurate. This stems from utilizing a monoenergetic gamma ray, versus beta counting for ^{32}S activation measurement.

Table 1. AFRRI-Reactor-Run Characteristics.

Run #	Exp. Room	Run Designation	Power Level (kW)	Run Duration (Sec.)
1	ER-1	6" Lead Wall / Cave	250	1800
2	ER-2	Free-Field	250	600
3	ER-1	Exercise Wheel	250	900
4	ER-1	Free-Field	250	600
5	ER-1	Phantom / 6" Lead Wall	500	1200

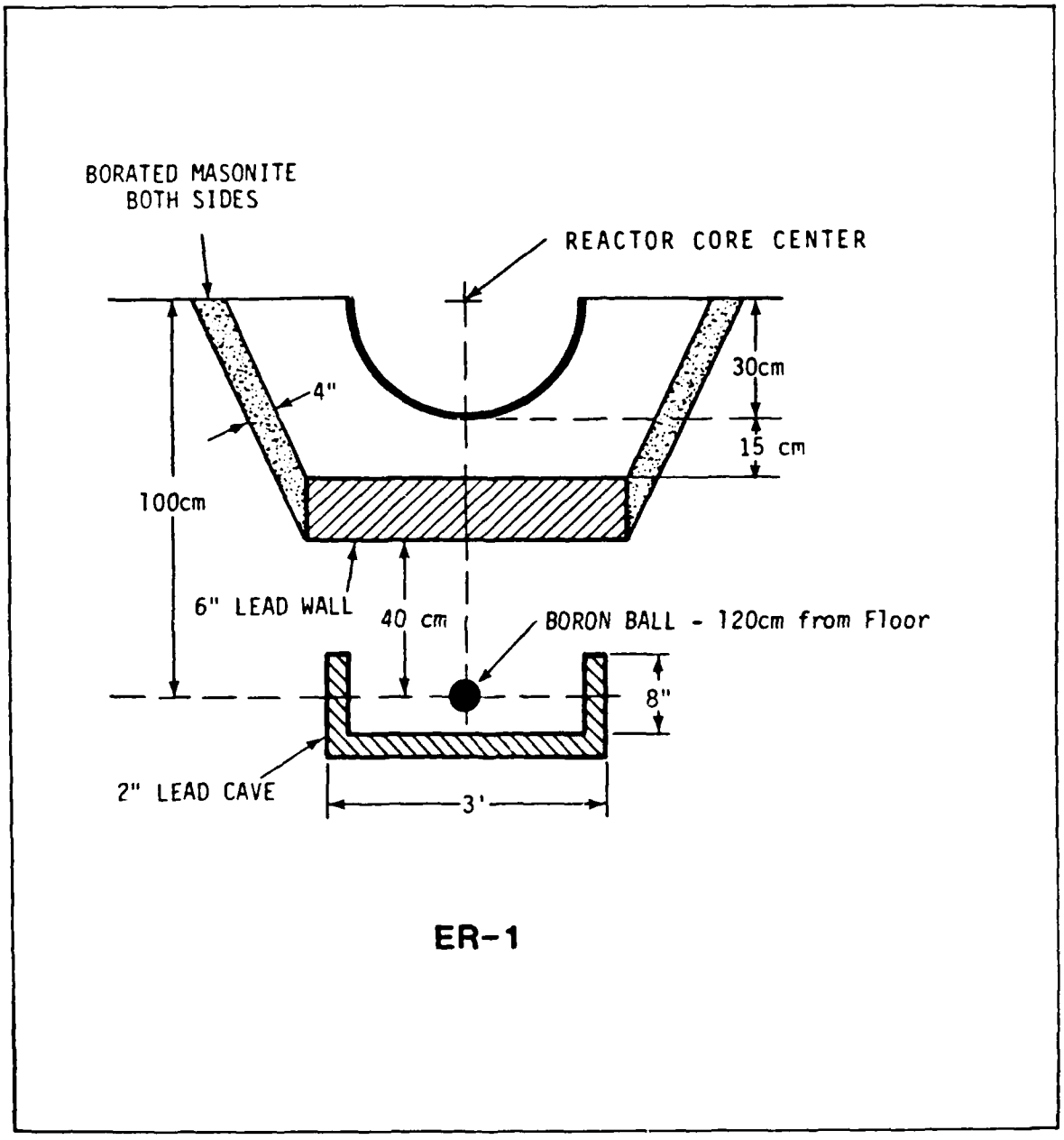

SAI-81CC-20.1

Figure 1. Top-view Schematic Diagram of AFRRI Reactor Run #1 (ER1 - 6" Lead Wall + 2" Lead Cave).

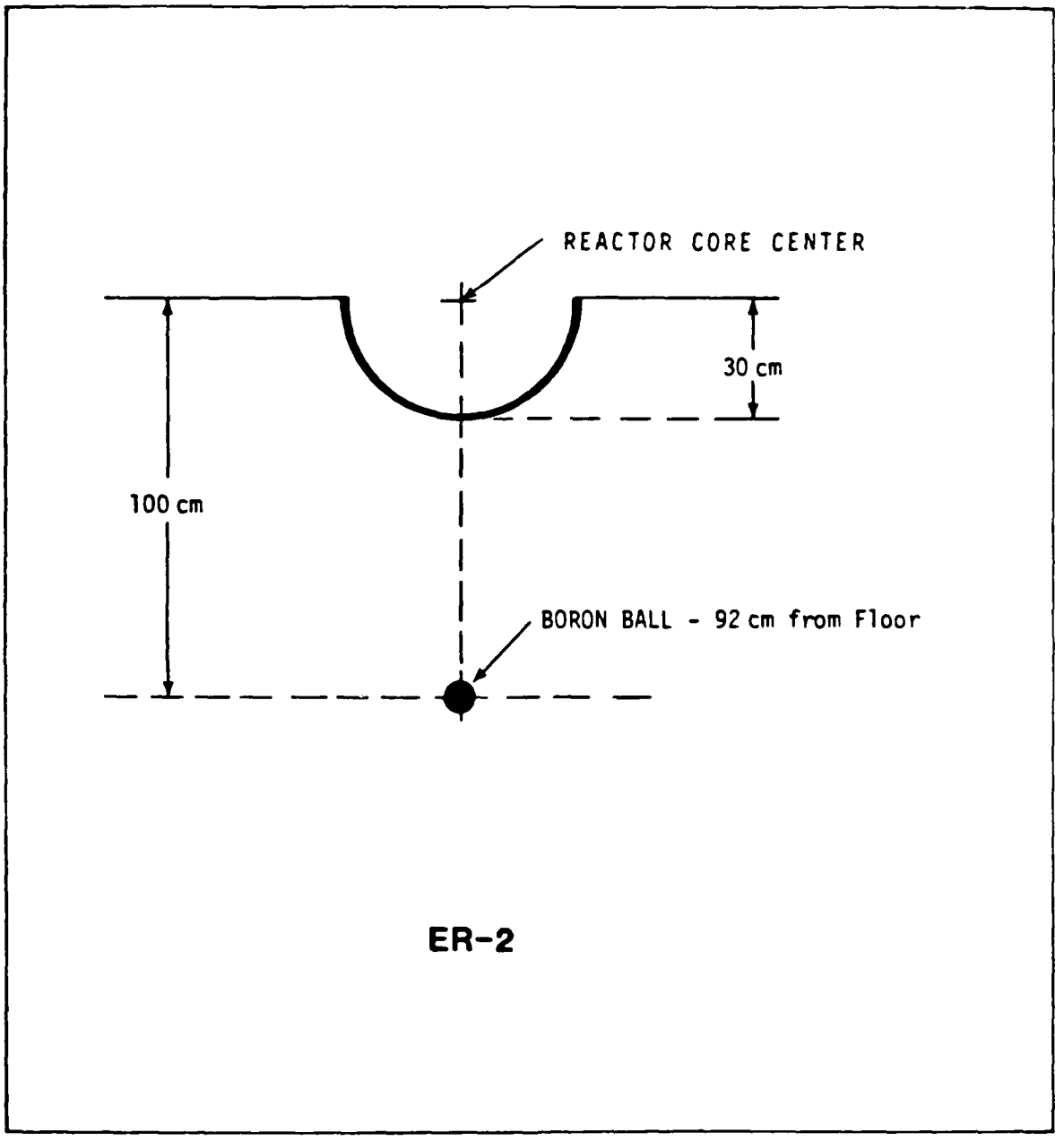

Figure 2. Schematic Diagram of AFRRI Reactor Run #2 (ER-2 Free Field). Top View.

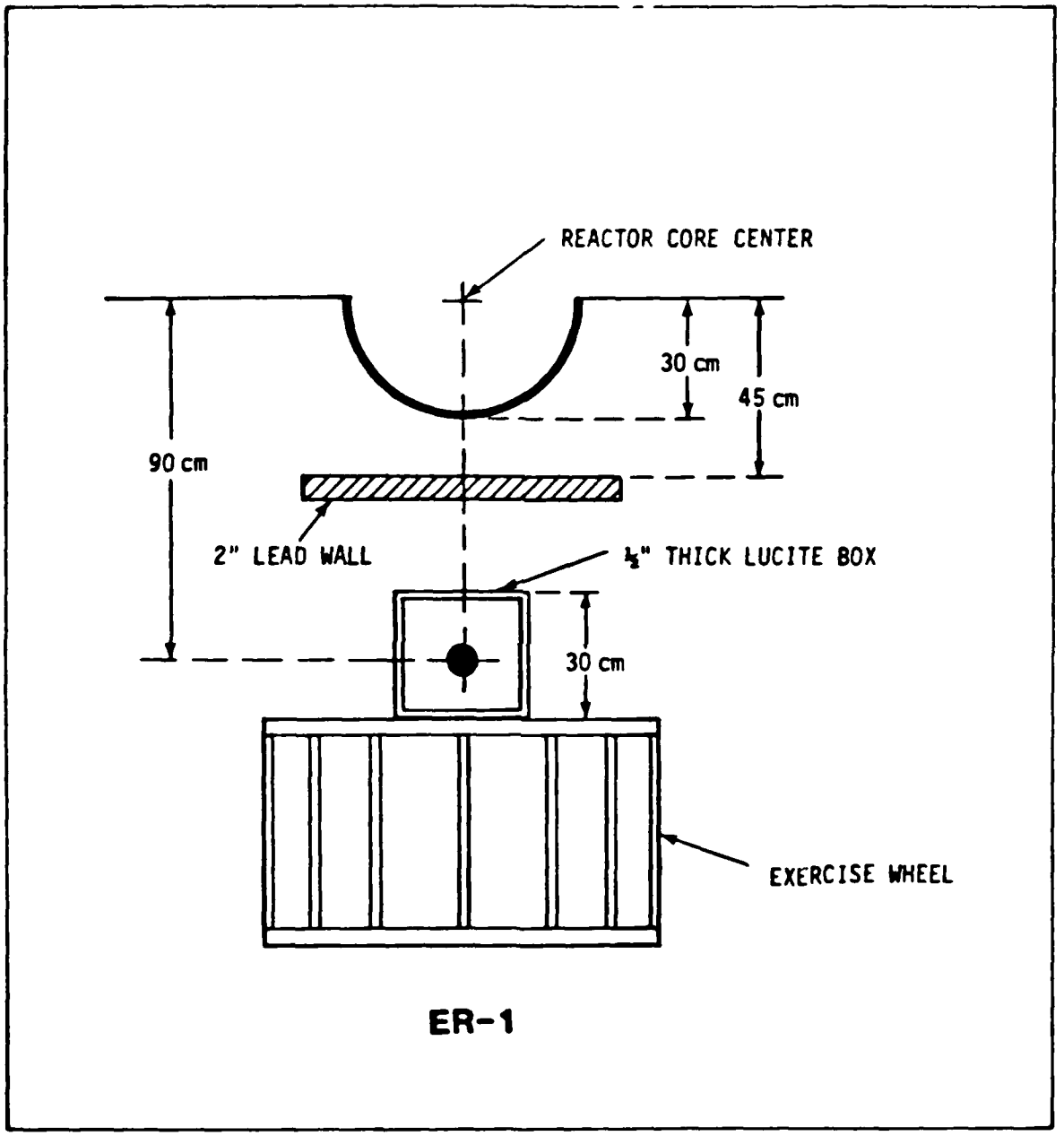

SAI-81cc-24

Figure 3. Schematic Diagram of AFRRI Reactor Run #3 (ER-1 EXERCISE WHEEL behind 2" Lead Wall). Top View.

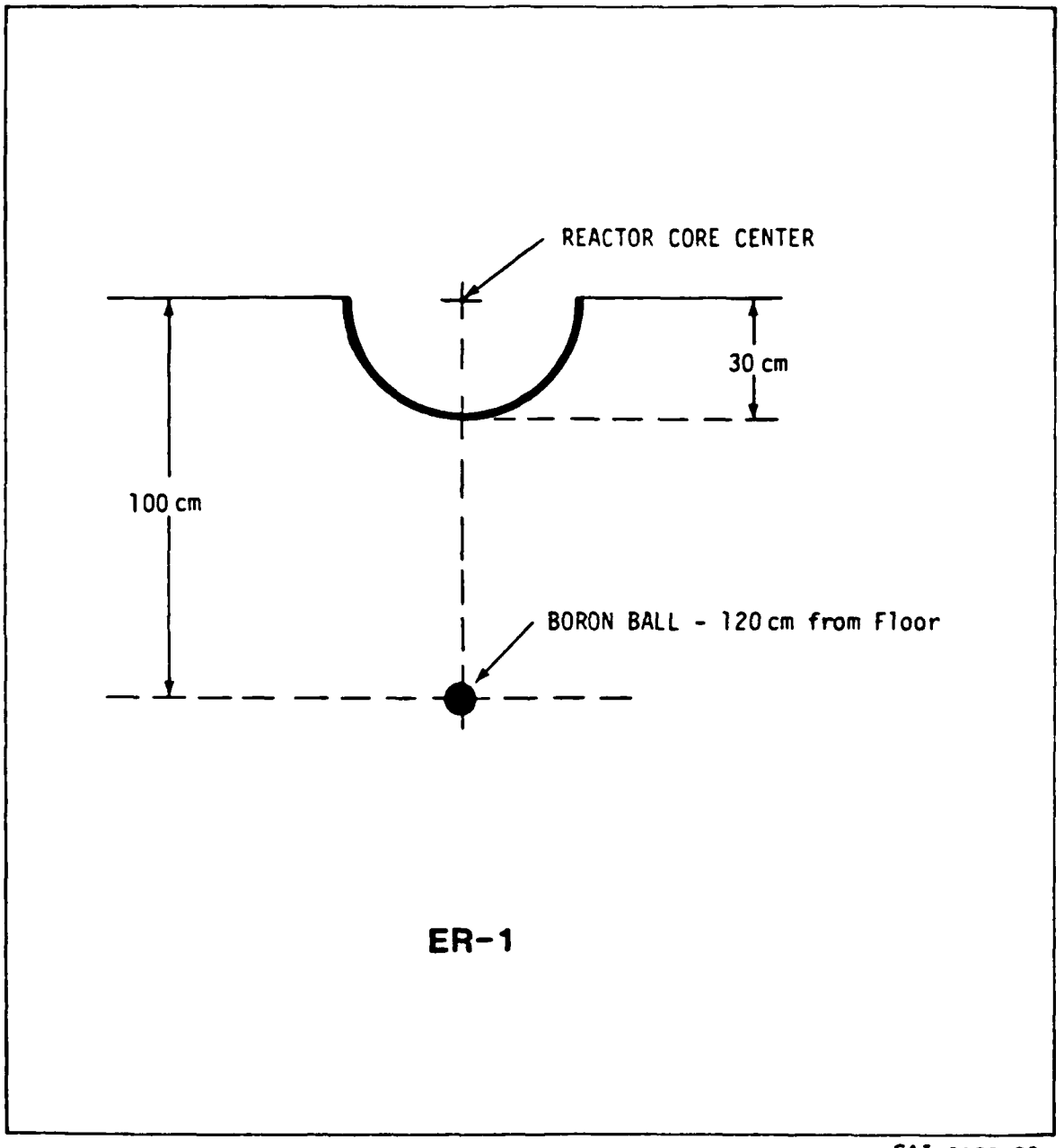

Figure 4. Schematic Diagram of AFRRI Reactor Run #4 (ER-1 Free Field). Top View.

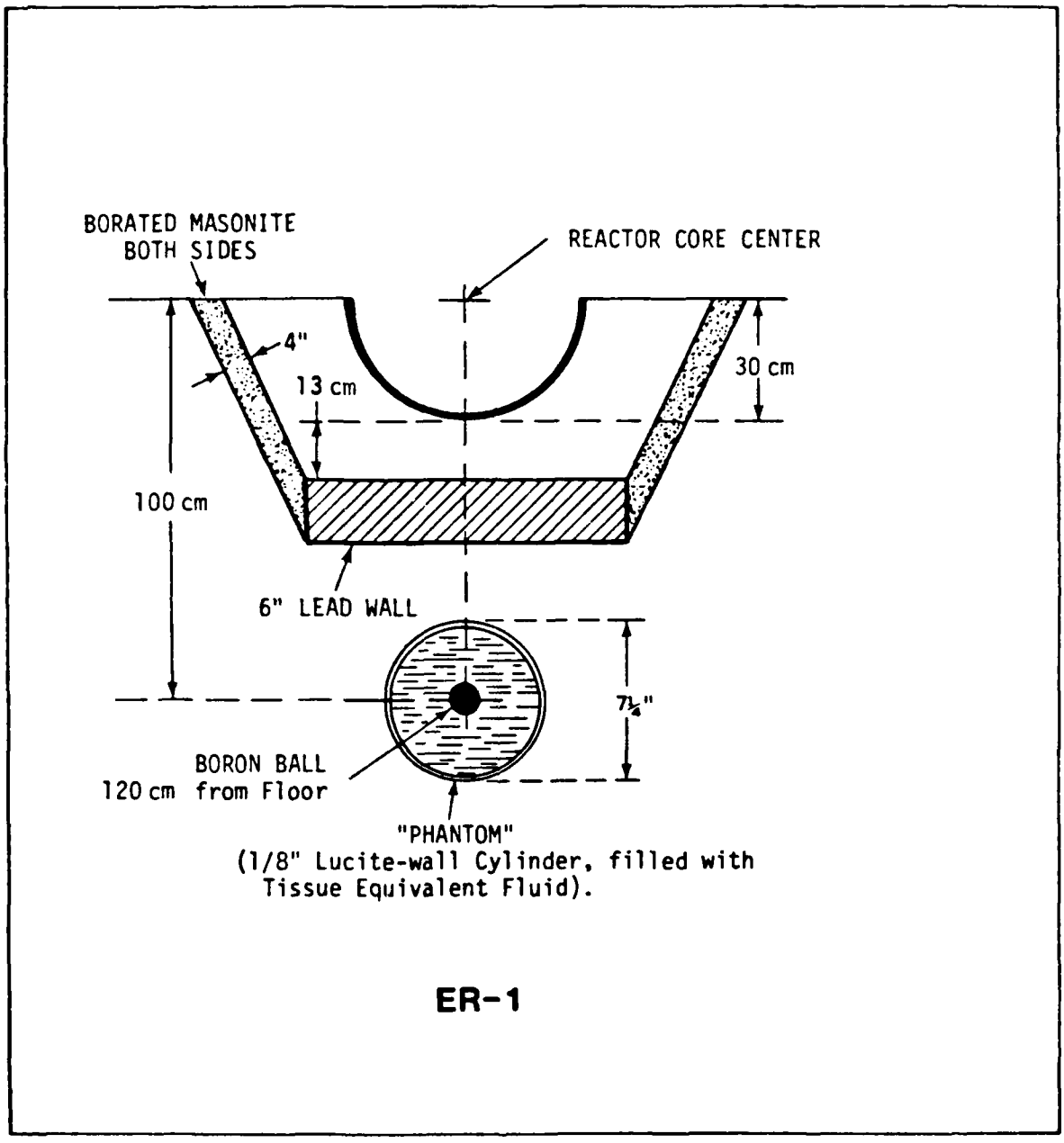

SAI-81CC-23.1

Figure 5. Top-view Schematic Diagram of AFRRI Reactor Run #5 (ER-1 "PHANTOM" behind 6" Lead Wall).

The AFRRI Ge(Li) detector was used for foil activation counting in two geometric configurations. The hotter foils were placed farther from the detector to eliminate excessive dead-time effects. The detector was calibrated for both geometries using an NBS eleven-line mixed radionuclide source. Some of the longer lived foils were counted at the SAI Ge(Li) detector.

The live-time for each foil count was accurately determined by using a calibrated pulser as the test input to the detector preamplifier: Any pulser event that occurred during the time the analyzer was busy or during incomplete recovery of the amplifier baseline from a previous gamma-ray pulse would cause the pulser pulse to lose a count in the (high resolution) peak.

At the conclusion of all foil counting the most active ^{235}U foil was used to determine the cascade correction to be applied on the fission foil activations as determined from the 537 and 1596 keV lines. The cascade effect for these particular gamma-rays is fully discussed in Ref. 1 and it affects the detector efficiency at these energies. Its determination consists of measuring the relevant count rates R_i at different distances from the detector face and plotting $1/\sqrt{R_i}$ as a function of distance d from the detector housing. The fractional difference of $1/\sqrt{R_i}$ at d = 0 (the surface of the detector cryostat), from the straight line plot for d > 0 values, gives a measure of the magnitude of the cascade correction for the particular detector used. It was found that this correction was of the order of 15% for the AFRRI Ge(Li) detector at 537 and 1596 keV.

The activations per nucleus induced in each foil were determined from the measured foil counts by the following equations

$$N = \frac{N_A \lambda t_i e^{\lambda t_w}(1-e^{-\lambda t_i})^{-1}(1-e^{-\lambda t_c})^{-1}}{\epsilon Y_f Y_\gamma N_0 m(a/A)} \qquad (1)$$

where N_A is the area of the gamma-ray peak

λ is the decay constant of the reaction

t_i is the irradiation time

t_w is the time interval between the end of irradiation and the beginning of counting

t_c is the foil count-time

ϵ is the detector efficiency

Y_γ is the gamma-ray yield per reaction

Y_f is the fractional fission yield (set this to unity for non-fission foils).

N_0 is Avogadro's number

m is the foil mass

a is the fractional natural abundance of the reactive isotope under consideration, and

A is the atomic weight of the foil element.

For the 1596 keV line of ^{140}La which is produced by the ^{140}Ba decays, Equation (1) becomes

$$N = \frac{N_A \lambda_B t_i (\lambda_L - \lambda_B) (1-e^{-\lambda_B t_i})^{-1} (1-e^{-\lambda_B t_c})^{-1}}{\lambda_L \varepsilon Y_\gamma^L Y_f (e^{-\lambda_B t_w} - e^{-\lambda_L t_w}) N_o m (a/A)} \qquad (2)$$

where the subscripts (superscripts) B and L refer to quantities associated with the ^{140}Ba and ^{140}La gammas respectively.

Finally, as a cursory check against possible errors in determining the number or activations per nucleus from Equations (1) and (2) above, the ratio N/N_{Ni} is determined for all foils in the reactor run under consideration, and compared to N/N_{Ni} from past experiments on file with similarly configured reactors. (Here, N_{Ni} is the number of activations per nucleus induced in the nickel foil by the reaction ($^{58}Ni(n, p)^{58}Co$).) In addition, this excercise provides first-hand qualitative information on the approximate shape of the neutron spectrum, prior to the final unfolding process which is discussed in the next section.

The foil activation data determined from reactor Runs 1 through 5 are presented in Table 2, and the unfolded spectra are shown in Figures 6 through 10.

Table 2. THRESHOLD FOIL ACTIVATIONS** FOR AFRRI TRIGA

Foil	Config.	E_{thr} (MeV)	λ (sec^{-1})	Run #1	Run #2	Run #3	Run #4	Run #5
^{197}Au	Boron	~ 0.01	2.976-6***	3.04-17	1.01-17	1.57-17	9.14-18	1.19-17
^{197}Au	Cadmium	$4x10^{-7}$	2.976-6	3.73-15	5.65-15	3.48-15	**	2.92-15
^{197}Au	Bare	0.0	2.976-6	4.52-15	5.24-15	5.06-15	2.81-15	1.34-14
^{55}Mn	Boron	~ 0.01	7.463-5	4.97-17	**	2.89-17	1.83-17	2.21-17
^{55}Mn	Cadmium	$4x10^{-7}$	7.463-5	1.29-15	7.31-16	9.01-16	5.52-16	6.76-16
^{55}Mn	Bare	0.0	7.463-5	2.73-15	8.88-15	5.83-15	1.22-15	3.30-14
^{235}U	Boron	~ 0.01	†	4.40-11	1.55-11	2.31-11	1.43-11	1.57-11
^{237}Np	Boron	0.5	†	2.65-11	**	1.63-11	1.13-11	8.83-12
^{115}In	Boron	1.0	4.279-5	1.02-16	6.86-17	7.63-17	6.62-17	3.71-17
^{238}U	Boron	1.45	†	3.17-12	2.50-12	2.97-12	2.21-12	1.42-12
^{232}Th	Boron	1.75	†	7.65-13	5.57-13	7.11-13	5.68-13	3.38-13
^{54}Fe	Boron	2.2	2.648-8	1.61-20	2.02-20	1.88-20	1.89-20	7.90-21
^{58}Ni	Boron	2.9	1.125-7	8.93-20	1.07-19	1.03-19	1.05-19	4.39-20
^{24}Mg	Boron	6.3	1.284-5	1.32-19	2.15-19	1.92-19	2.15-19	9.30-20
^{56}Fe	Boron	7.5	7.463-5	5.22-19	8.82-19	7.68-19	8.23-19	3.51-19
^{27}Al	Boron	8.7	1.284.5	6.52-20	1.06-19	9.57-20	9.98-20	4.65-20
^{90}Zr	Boron	14.0	2.456-6	2.95-21	4.02-21	4.07-21	4.03-21	2.18-21

* Activations are given as $N \cdot sec^{-1} \cdot atom^{-1}$, except for fission foils, where $N \cdot atom^{-1}$ is given. N is the gamma-ray emission rate per atom.

** Aborted readings (inconsistent with the other foils).

*** Read as 2.976×10^{-6}.

† The ^{140}Ba, ^{97}Zr, and ^{140}La lines are used in conjunction with the fission foils, except for ^{232}Th, where ^{140}La cannot be used.

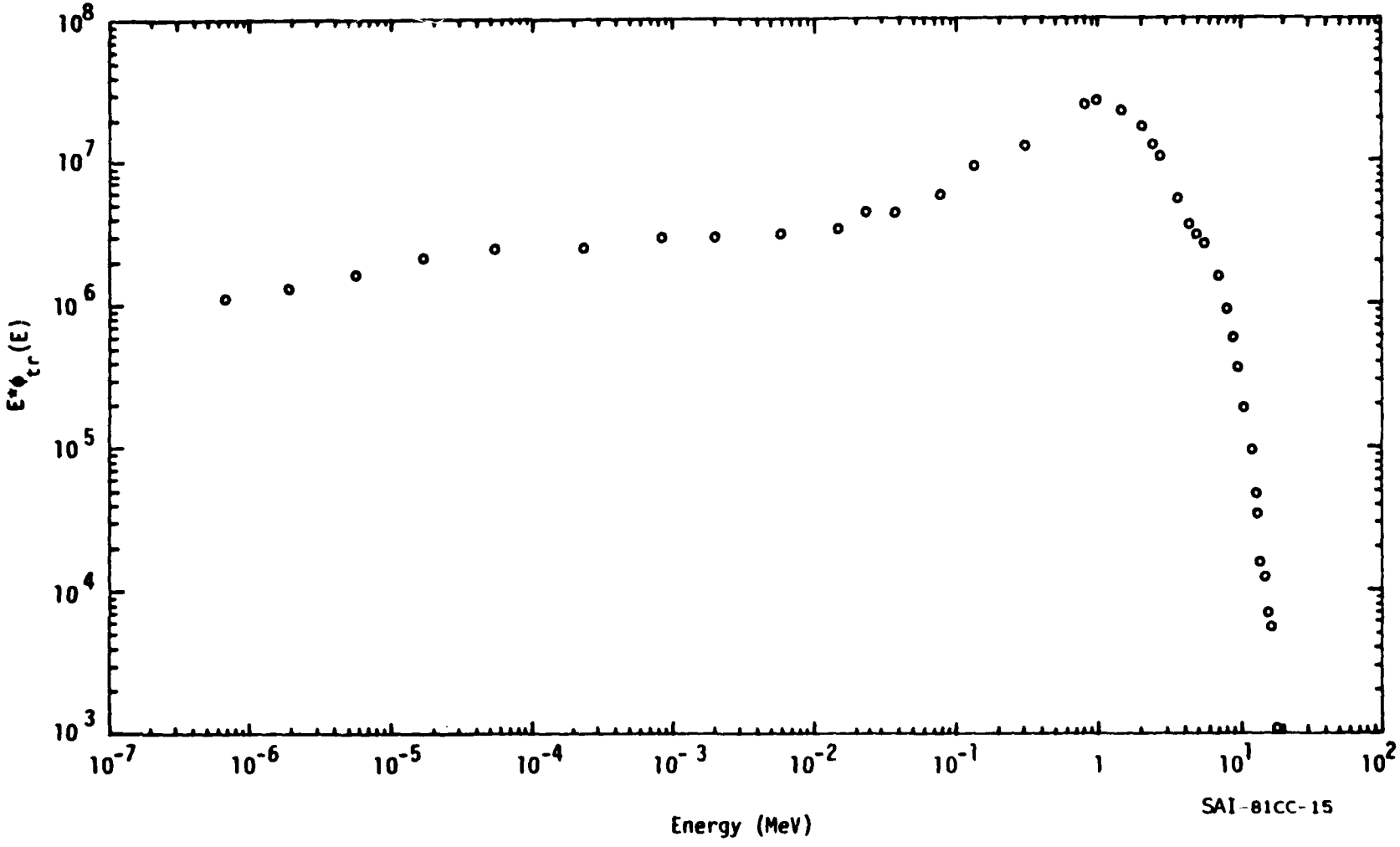

Figure 6. $E*\phi_{tr}(E)$ for AFRRI Reactor Run #1 (6" Pb Wall + 2" Pb Cave).

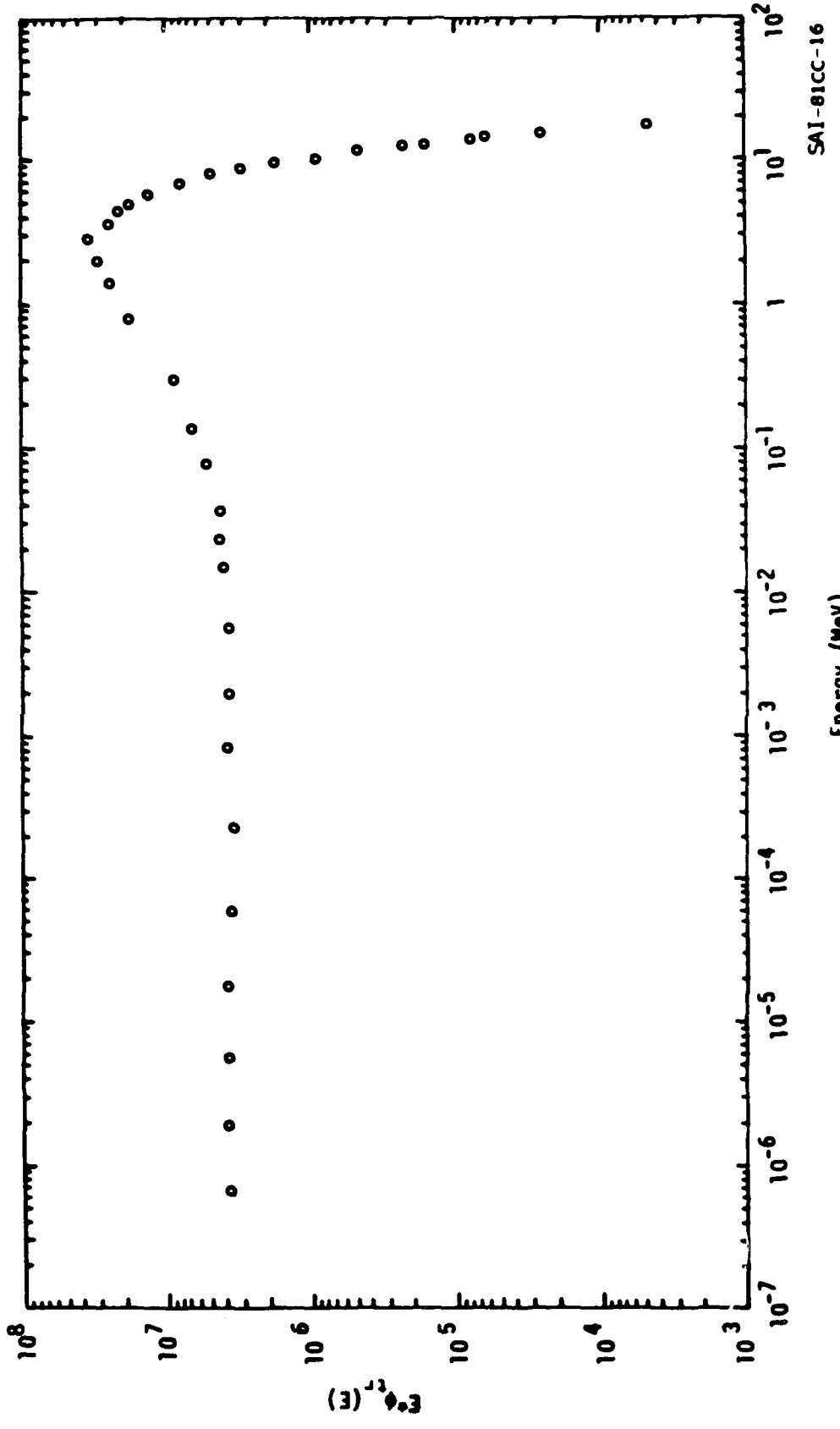

Figure 7. $E*\phi_{tr}(E)$ for AFRRI Reactor Run #2 (ER-2 Free Field).

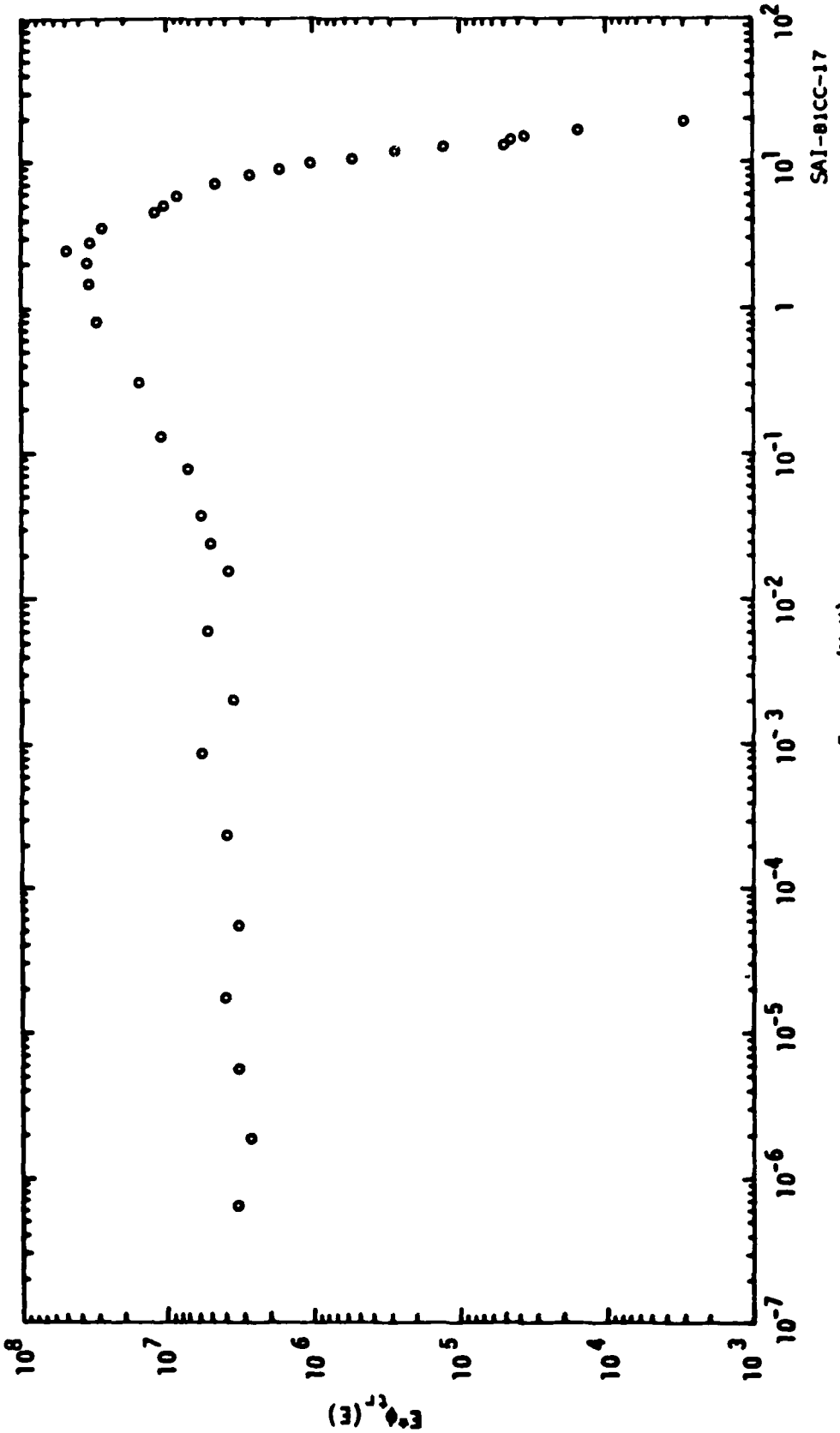

Figure 8. $E*\phi_{tr}(E)$ for AFRRI Reactor Run #3 (Exercise Wheel behind 2" Pb Wall).

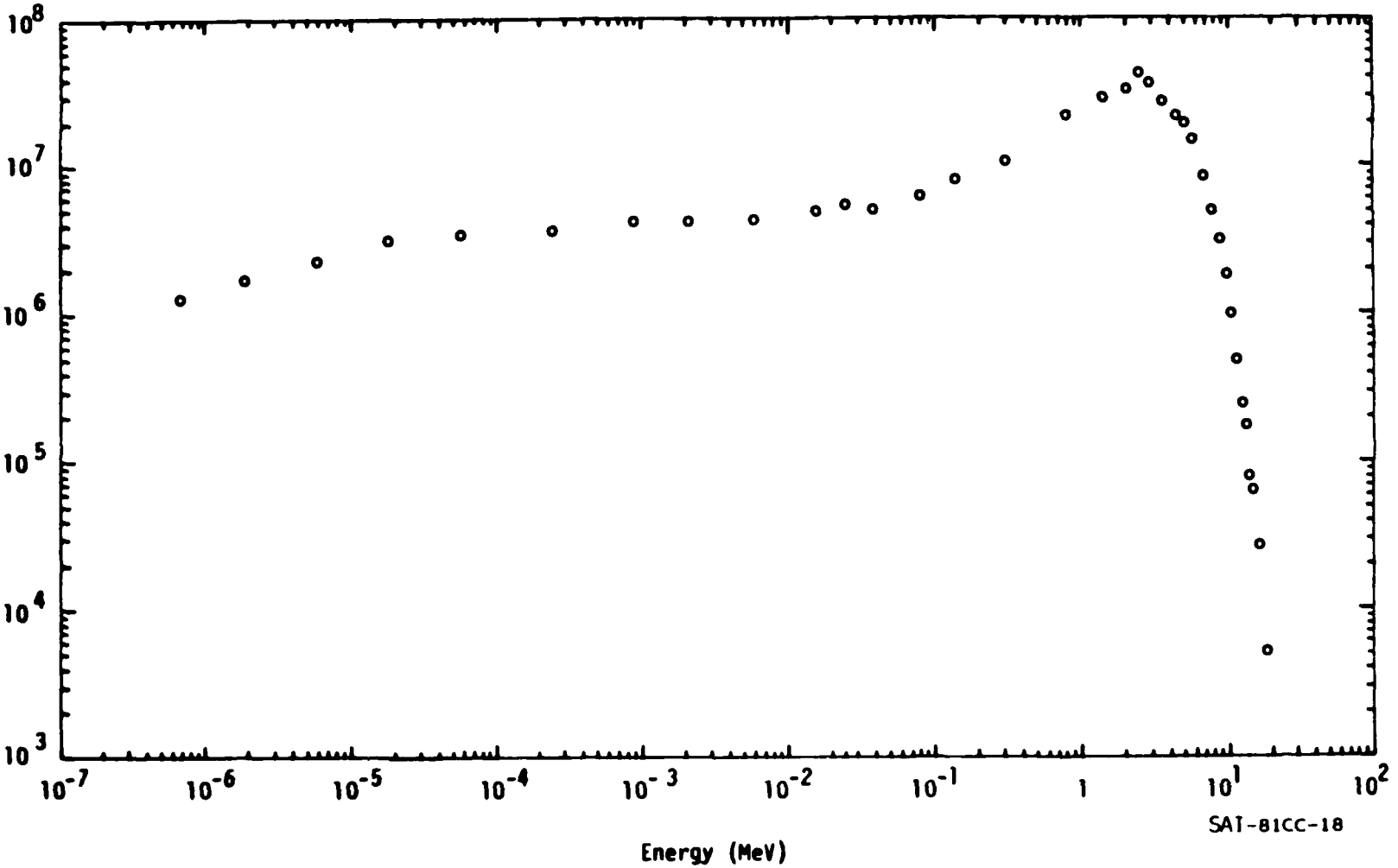

Figure 9, $E*\phi_{tr}(E)$ for AFRRI Reactor #4 (ER-1 Free Field).

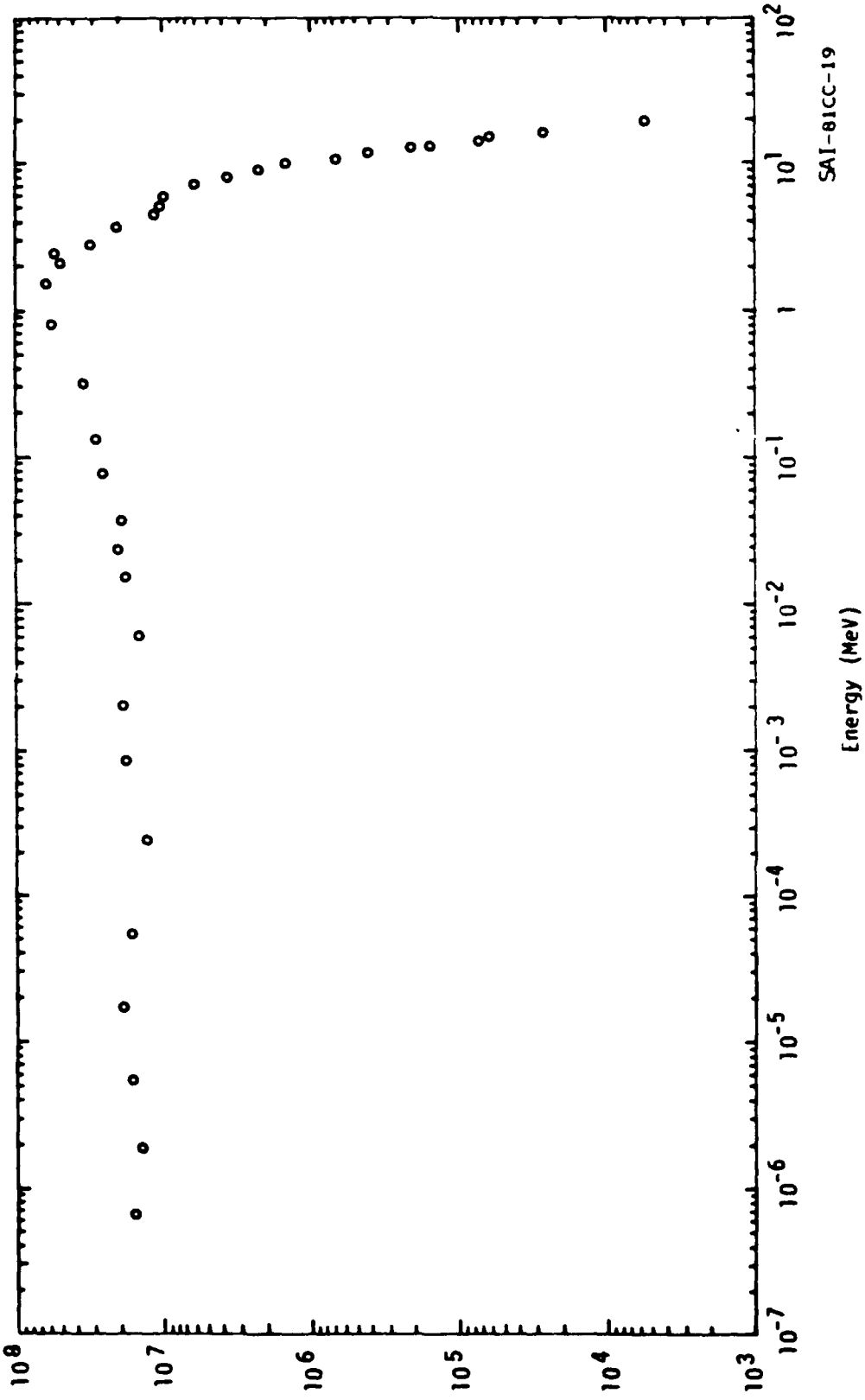

Figure 10. $E*\phi_{tr}(E)$ for AFRRI Reactor #5 (Phantom behind 6" Pb Wall).

2.2 Results: Shape-Comparison Between Measured and Calculated (Trial) Spectra

The unfolded neutron spectra resulting from the measured activations are shown in Figures 11 through 15 for reactor Runs 1 through 5, respectively. Also shown are the calculated spectra for the same reactor configurations, which were used as the input trial for the SAND II code. For shape comparison the measured and calculated spectra are normalized so that best fit is obtained for the energy region above $E_n \simeq 0.2$ MeV, which is the effective threshold for semiconductor neutron damage. The measured spectra are normalized to unit fluence above 10 keV.

With regard to the calculated trial spectra it must be noted that both one-dimensional and three-dimensional transport codes were utilized in modeling the actual experimental conditions. In Runs 1, 2 and 4 the one-dimensional models were found to be adequate as trial spectra in the unfolding code.

For reactor Run #3 (exercise wheel behind 2" Pb shield) and Run #5 (phantom behind 6" Pb shield), it was found that a mixed 1-D/3-D trial spectrum produced much better shape agreement with the measured ones than either the 1-D or 3-D spectrum alone. The "mixing" was accomplished by splicing the high energy part ($E \gtrsim 4$MeV) of the 1-D calculation to the 3-D calculation part with $E < 4$ MeV, where the latter does not suffer much due to the statistical uncertainity. The need for a spliced spectrum trial spectrum in Run 3 (2" Pb wall and activity wheel) and Run 5 (phantom behind 6" Pb shield) appears due to a combination of reasons. The complex geometry of the activity wheel and the large thermalizing power and capture properties of the lucite wheel and tissue-equivalent phantom required the need for the 3-D calculations. Unfortunately, as stated above, the statistical uncertainty of the high energy groups in the 3-D spectra required replacement by the 1-D spectra. Volume II of this report contains further discussion of the 3-D and spliced calculations.

It is seen that the calculated and the measured spectra for reactor Runs 1 through 4 agree quite well in shape: It took no more than two iterations for the unfolding code to reach the required 5% deviation between measured and calculated foil activations.

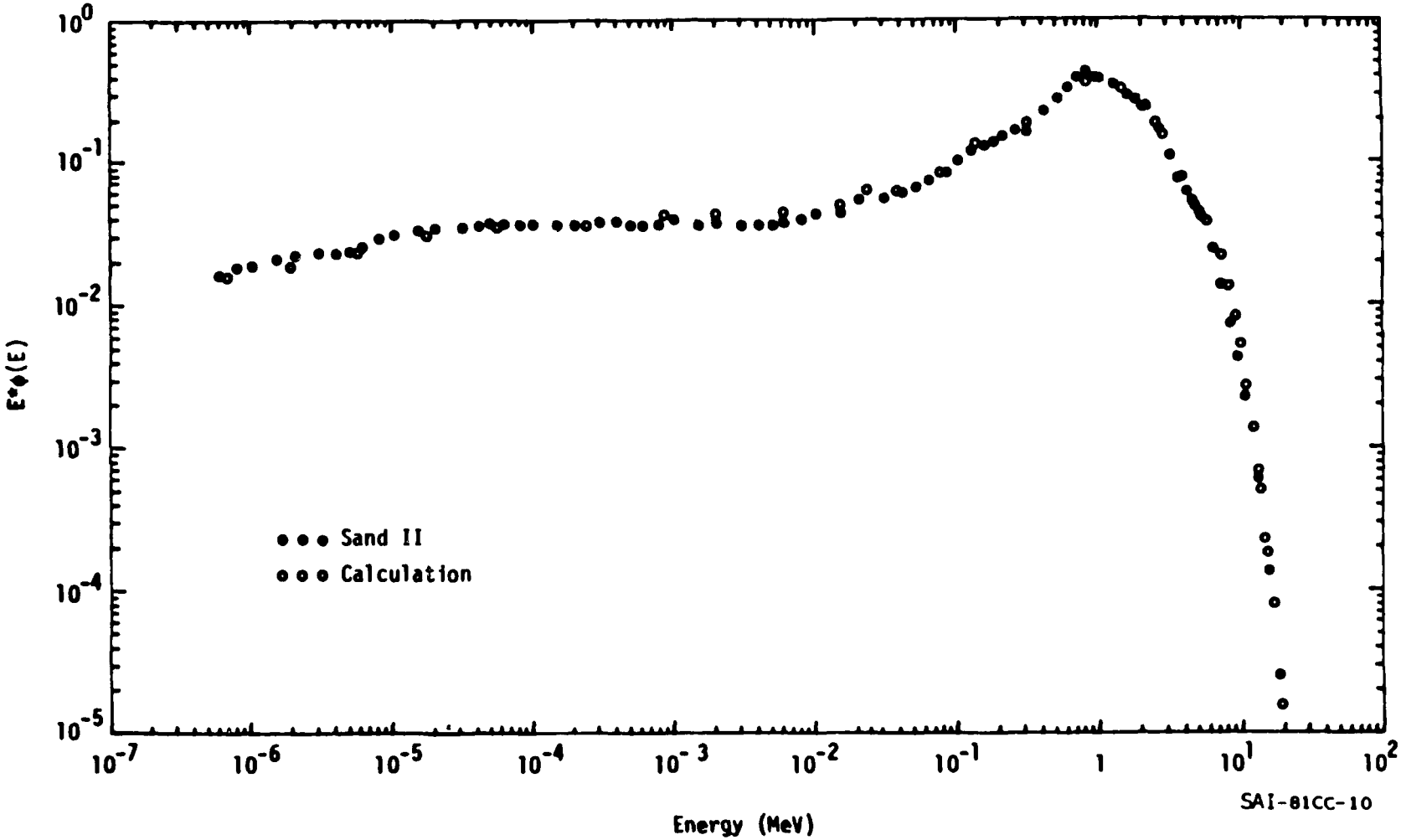

Figure 11. Shape Comparison of Calculated and Measured Spectra for AFRRI Run #1 (6" Pb Wall + 2" Pb Cave).

The measured data were normalized to unit flux above 10 keV and the calculated data normalized to the measured data above 0.2 meV, the "threshold" for radiation damage to silicon.

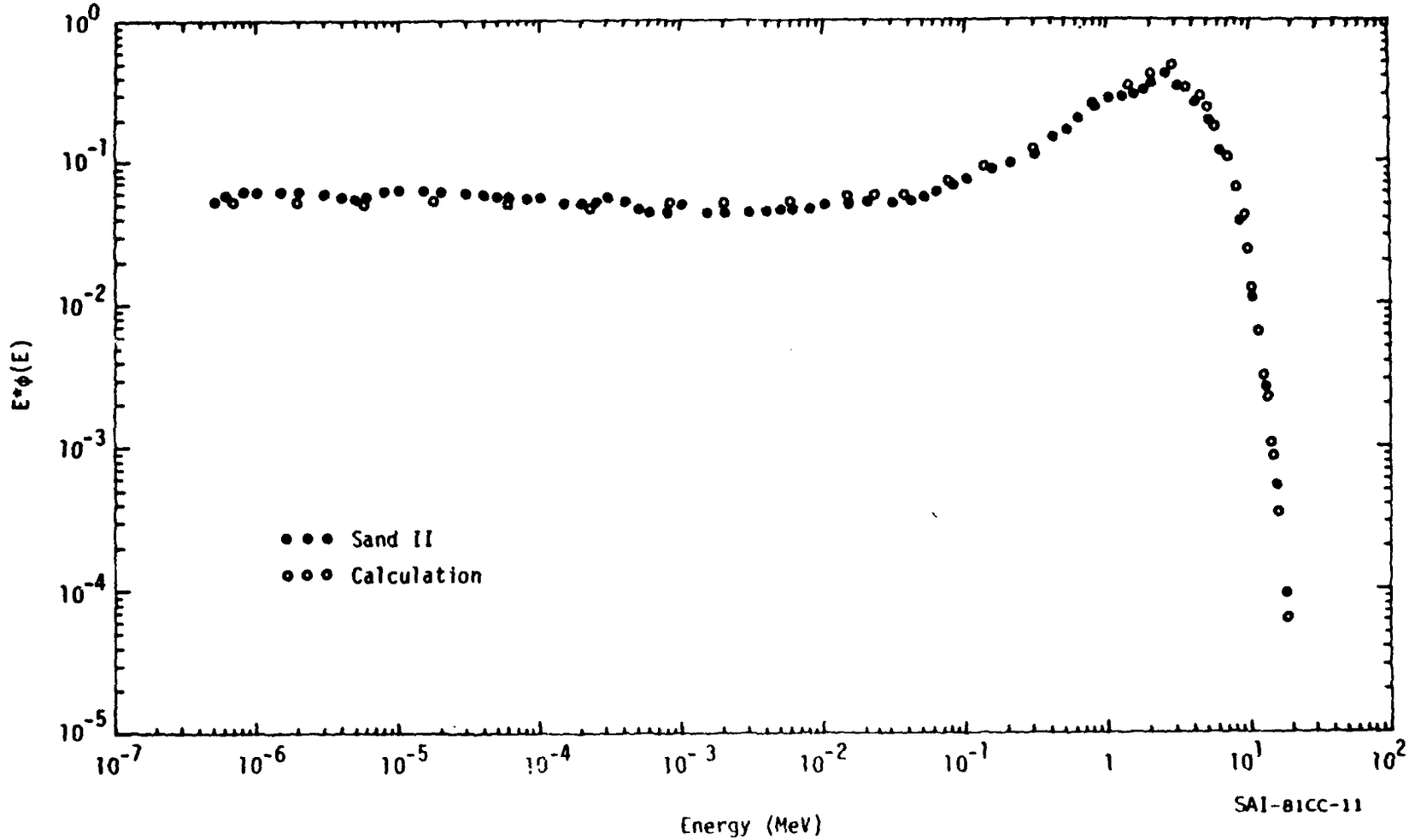

Figure 12. Shape Comparison of Calculated and Measured Spectra for AFRRI Run #2 (ER-2 Free Field). The measured data were normalized to unit flux above 10 keV and the calculated data normalized to the measured data above 0.2 meV, the "threshold" for radiation damage to silicon.

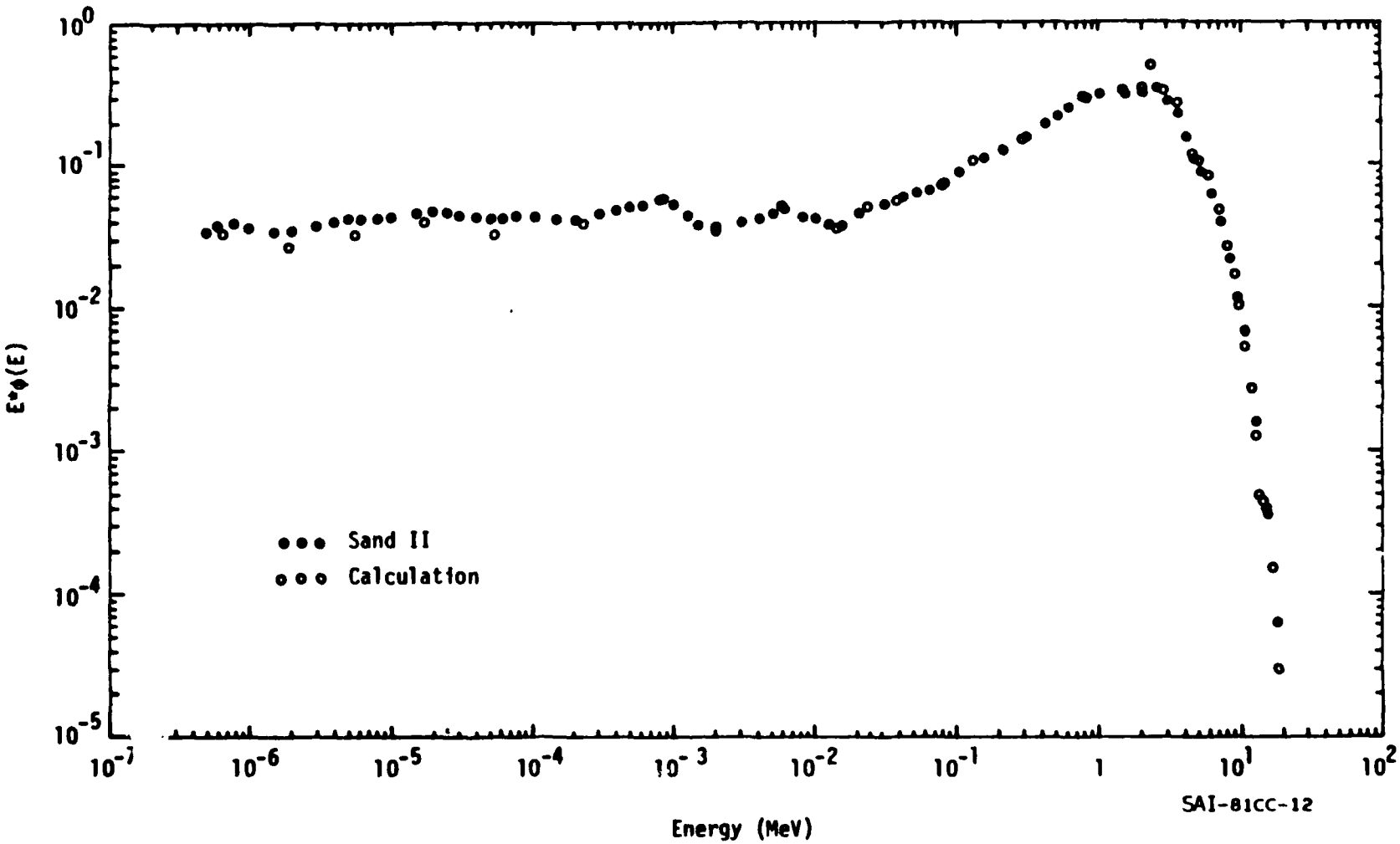

Figure 13. Shape Comparison of Calculated and Measured Spectra for AFRRI Run #3 (Exercise Wheel behind 2" Pb Wall).
The measured data were normalized to unit flux above 10 keV and the calculated data normalized to the measured data above 0.2 meV. the "threshold" for radiation damage to silicon.

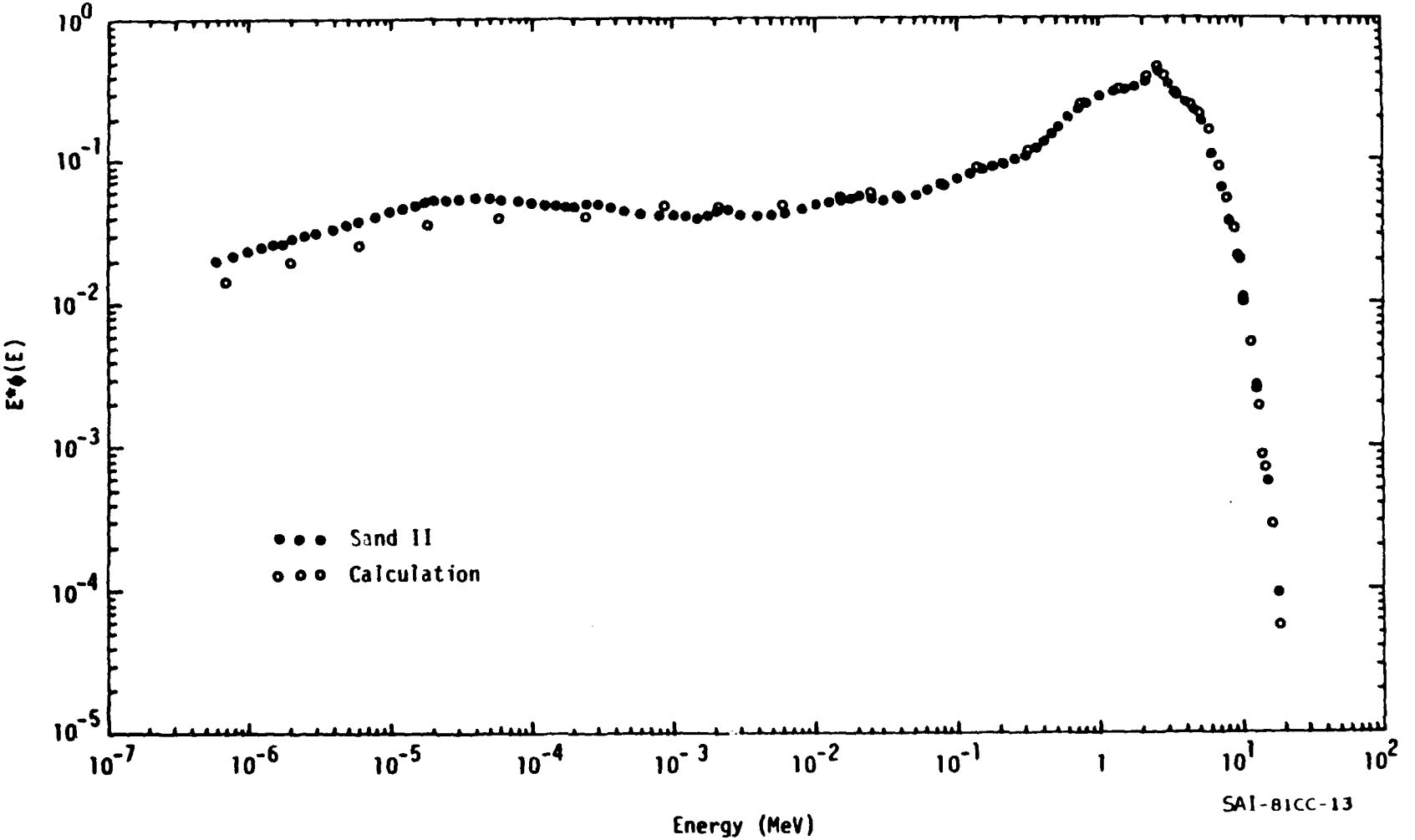

Figure 14. Shape Comparison of Calculated and Measured Spectra for AFRRI Run #4 (ER-1 Free Field). The measured data were normalized to unit flux above 10 keV and the calculated data normalized to the measured data above 0.2 meV, the "threshold" for radiation damage to silicon.

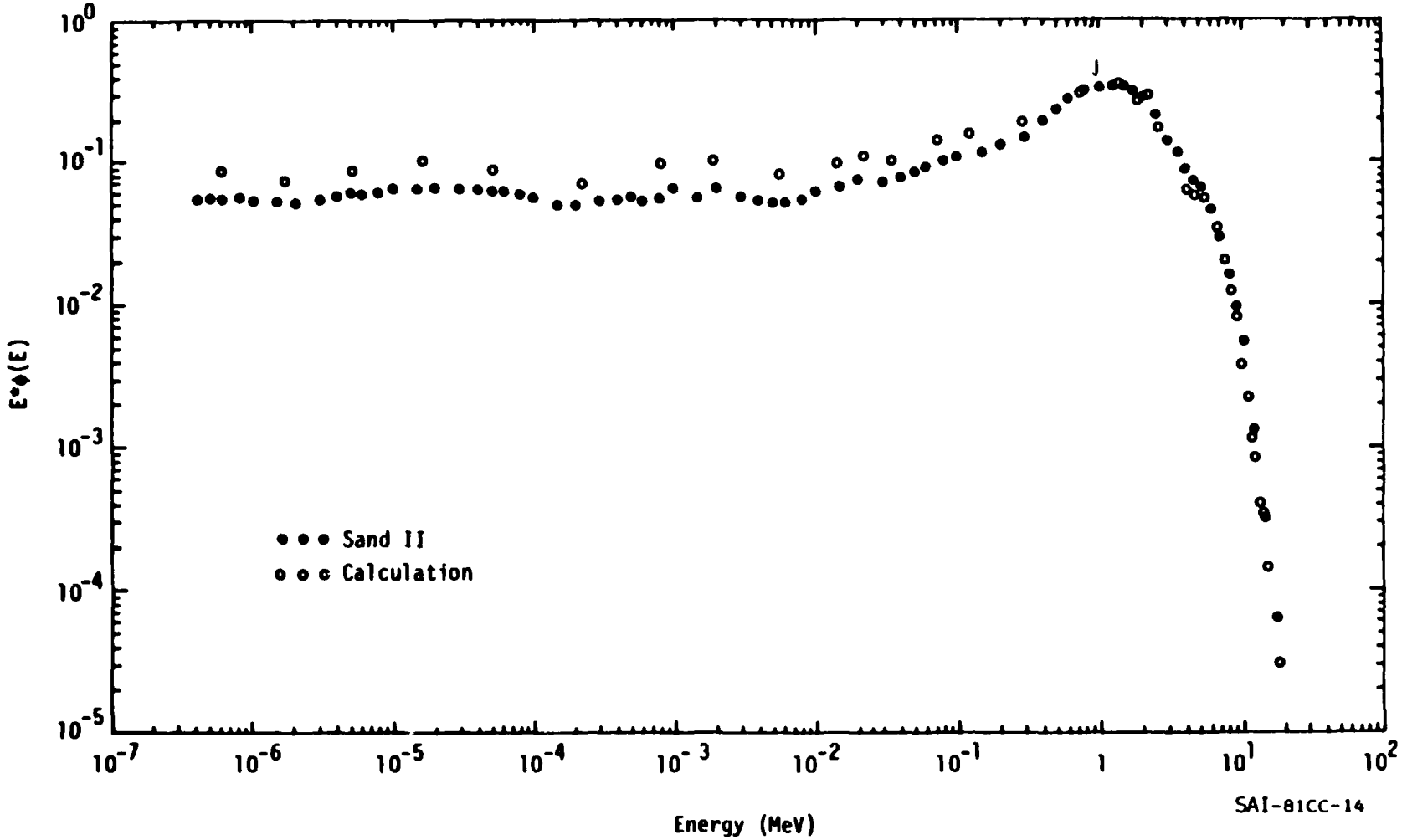

Figure 15. Shape Comparison of Calculated and Measured Spectra for AFRRI Run #5 (Phantom behind 6" Pb Wall).
The measured data were normalized to unit flux above 10 keV and the calculated data normalized to the measured data above 0.2 meV, the "threshold" for radiation damage to silicon.

In reactor Run 5 (Phantom), the measured and calculated spectra do not agree well in shape in that the calculation yields about a 50% excess in the 1/E region of the spectrum (below 0.3 MeV). As mentioned above, the calculated spectrum for this case is a mixture of a one-dimensional and a three-dimensional calculation joined at E_n = 4.07 MeV. In the neighborhood of this energy, the 3-D calculation still suffers from statistical uncertainties. Thus, the lack of shape agreement in this case is at least partly due to difficulties in accurate normalization between the two calculations at their juncture point.

The tabulated spectra for Runs 1 through 5 are presented in Table 3. These data represent the absolute flux, per kilowatt, for the calculated data as well as for the measurements: There is no normalization to the measured data above 0.2 MeV, as in Figures 11 through 15, so that direct comparisons can be made as to predicted group flux per kilowatt.

Table 3. E*φ(E) Calculated and Measured Neutron Flux Per Group Per Kilowatt for AFRRI Runs 1-5.

		RUN #1		RUN #2		RUN #3		RUN #4		RUN #5	
Group #	Eupper (MeV)	φ Calc	φ Meas.	φ Calc	φ Meas.	φ Calc	φ Meas.	φ Calc	φ Meas.	φ Calc	φ Meas.
1	19.6	1.57+2	1.38+02	6.99+2	5.22+02	4.37+2	3.55+02	7.34+2	5.22+02	8.34+1	8.26+01
2	16.9	6.90+2	8.63+02	3.16+3	3.37+03	1.74+3	2.25+03	3.34+3	3.39+03	3.40+2	4.92+02
3	14.9	6.31+2	7.05+02	2.98+3	2.84+03	1.79+3	1.85+03	3.15+3	2.85+03	2.98+2	3.89+02
4	14.2	4.40+2	5.31+02	2.12+3	2.20+03	1.26+3	1.42+03	2.25+3	2.20+03	2.04+2	2.89+02
5	13.8	2.54+2	2.68+03	1.23+4	1.12+04	7.29+3	7.28+03	1.30+4	1.12+04	1.16+3	1.45+03
6	12.8	2.20+3	2.28+03	1.09+4	1.02+04	6.48+3	6.55+03	1.15+4	1.01+04	1.02+3	1.28+03
7	12.2	8.75+3	6.29+03	4.36+4	3.16+04	2.55+4	1.93+04	4.65+4	3.01+04	3.75+3	3.66+03
8	11.1	1.87+4	1.39+04	9.31+4	6.98+04	5.48+4	4.23+04	9.92+4	6.64+04	8.10+3	7.99+03
9	10.0	3.47+4	2.58+04	1.74+5	1.30+05	9.98+4	7.73+04	1.84+5	1.23+05	1.45+4	1.44+04
10	9.05	5.62+4	4.25+04	2.85+5	2.16+05	1.67+5	1.29+05	3.05+5	2.08+05	2.28+4	2.27+04
11	8.19	9.05+4	6.85+04	4.56+5	3.47+05	2.59+5	2.01+05	4.91+5	3.34+05	3.56+4	3.53+04
12	7.41	2.24+5	1.75+05	1.12+6	8.76+05	6.81+5	5.11+05	1.22+6	8.40+05	8.91+4	8.69+04
13	6.38	6.47+5	6.27+05	3.40+6	2.95+06	2.04+6	1.49+06	3.69+6	2.78+06	2.48+5	2.59+05
14	4.97	1.48+5	1.79+05	8.93+5	8.49+05	5.38+5	4.07+05	9.75+5	8.02+05	5.83+4	6.83+04
15	4.72	5.02+5	6.09+05	2.99+6	2.79+06	1.79+6	1.40+06	3.29+6	2.66+06	1.78+5	2.16+05
16	4.07	1.54+6	1.94+06	7.12+6	6.87+06	8.30+6	5.65+06	7.96+6	6.64+06	5.31+5	6.97+05
17	3.01	2.49+6	2.78+06	7.56+6	7.03+06	7.69+6	6.07+06	8.49+6	6.80+06	6.82+5	8.37+05
18	2.39	4.42+5	5.21+05	1.26+6	1.15+06	1.62+6	1.15+06	1.39+6	1.11+06	1.82+5	1.92+05
19	2.31	3.96+6	4.37+06	6.72+6	6.58+06	7.92+6	6.40+06	7.68+6	6.44+06	1.20+6	1.33+06
20	1.83	1.07+7	1.27+07	1.24+7	1.18+07	1.69+7	1.27+07	1.43+7	1.19+07	3.10+6	3.22+06
21	1.11	1.75+7	2.08+07	1.25+7	1.27+07	2.11+7	1.58+07	1.47+7	1.25+07	4.00+6	4.03+06
22	5.50-1	1.63+7	1.86+07	1.12+7	1.18+07	2.01+7	1.60+07	1.33+7	1.08+07	4.51+6	3.71+06
23	1.58-1	3.21+6	3.41+06	2.34+6	2.33+06	3.85+6	3.03+06	2.80+6	2.23+06	9.78+5	7.53+05
24	1.11-1	4.33+6	4.85+06	3.87+6	3.86+06	5.32+6	4.49+06	4.63+6	3.70+06	1.91+6	1.39+06
25	5.25-2	3.21+6	3.54+06	3.07+6	3.10+06	4.46+6	3.48+06	3.66+6	3.02+06	1.39+6	1.06+06
26	2.48-2	5.45+5	5.75+05	5.08+5	4.83+05	6.00+5	5.10+05	6.58+5	5.27+05	2.41+5	1.76+05
27	2.19-2	2.52+6	2.78+06	3.07+5	2.99+06	2.77+6	2.41+06	3.70+6	2.94+06	1.35+6	9.63+05
28	1.03-2	3.45+6	3.39+06	4.32+6	4.05+06	5.96+6	4.06+06	5.10+6	3.59+06	1.72+6	1.14+06
29	3.35-3	2.99+6	2.97+06	3.77+6	3.56+06	3.50+6	3.08+06	4.30+6	3.27+06	1.87+6	1.14+06
30	1.23-3	2.22+6	2.21+06	2.83+6	2.68+06	4.40+6	3.20+06	3.16+6	2.37+06	1.33+6	8.24+05
31	5.83-4	4.87+6	5.21+06	6.70+6	7.16+06	7.47+6	6.50+06	7.09+6	6.41+06	2.61+6	1.74+06
32	1.01-4	3.17+6	3.59+06	4.82+6	5.60+06	4.36+6	4.43+06	4.56+6	5.02+06	2.20+6	1.46+06
33	2.90-5	2.21+6	2.71+06	3.88+6	4.89+06	4.12+6	3.83+06	3.26+6	3.76+06	1.92+6	1.24+06
34	1.07-5	2.20+6	2.60+06	4.88+6	5.80+06	4.43+6	4.33+06	3.00+6	3.48+06	2.12+6	1.44+06
35	3.06-6	1.40+6	1.72+06	3.90+6	4.85+06	2.82+6	2.83+06	1.77+6	2.11+06	1.43+6	9.98+05
36	1.13-6	1.15+6	1.36+06	3.90+6	4.69+06	3.44+6	3.08+06	1.35+6	1.50+06	1.70+6	1.08+06
37*	4.14-7	2.79+6	2.63+6	3.37+7	5.59+7	5.55+7	2.06+7	3.34+6	3.61+6	1.02+8	5.58+7

* The measured thermal neutron flux was determined from the bare and cadmium covered ^{197}Au and ^{55}Mn threshold foils (cadmium-difference measurements).

3.0 BROAD-GROUP COMPARISON BETWEEN MEASUREMENTS AND CALCULATIONS

The measured neutron spectra shown in Figures 11 thourgh 15 were regrouped in the same 37 energy-group structure as the calculations for point-by-point comparison. The results are presented in Table 3. The absolute measured and calculated data are shown; i.e., no normalization was employed here. The calculations can most meaningfully be compared to the measured data in the 0.1 to 7 MeV energy region, where most of the biological dose/silicon damage occurs.

Table 4 presents measured and calculated fluxes above 10 keV, above the cadmium cutoff (0.4 eV), and for the thermal group (below 0.4 eV). Agreement is excellent for ER-2 free field and is good for the 6" Pb plus 2" cave. In all cases except Run 5 (phantom behind 6" of lead) agreement between the measured versus calculated fast and epicadmium fluxes (ratios between measured groups 1-27 and 1-36 and the corresponding calculated groups) is quite good. In a similar fashion the agreement between measured and calculated thermal fluxes is poor when compared to the agreement between the fast and the epicadmium-region fluxes. It is to be noted that the spliced 1-D/3-D spectra, (Runs 3 and 5) have the greatest differences. These differences may, in part, be ascribed to a renormalization difference between the 1-D and 3-D calculations. In general the calculation of thermal neutron flux is far more complicated than for fast neutrons because thermal neutrons are very sensitive to the thickness and location of all scattering materials, moderating materials (wood, plastic, concrete etc.), and of the thermal neutron absorbers.

4.0 SPECTRUM TAILORING WITH THE AFRRI NEUTRON FIELD

In comparing the measured free field flux (Run #4, ER-1) and the flux behind the 6" lead wall with 2" lead cave (Run #1), note that the flux is higher behind the 6" lead wall with 2" lead cave than in front of the wall (Run #4 free field) in the 0.1 to 1.0 MeV energy region. Above 1 MeV, the flux behind the wall is appreciably lower. A comparison of the spectral shapes of Figures 11 (6" Pb and cave) and 12 (free field) shows the reason

Table 4. Absolute Comparison Between Calculated and Measured Flux Per Kilowatt for Three Spectral Regions.

Run #	Groups 1-27 (E_n > 10 keV)		Groups 1-36 (Epicadmium Region)		Group 37 (Thermal Region)	
	ϕ Calc.	ϕ Meas.	ϕ Calc.	ϕ Meas.	ϕ Calc.	ϕ Meas.
1	6.85+7	7.88+7	9.22+7	1.04+8	2.79+6	2.63+6
2	7.83+7	7.89+7	1.17+8	1.22+8	3.37+7	5.59+7
3	1.06+8	8.20+7	1.47+8	1.18+8	5.55+7	2.06+7
4	9.86+7	7.66+7	1.32+8	1.08+8	3.34+6	3.61+6
5	2.08+7	1.91+7	3.77+7	3.02+7	1.02+8	5.58+7

for this: The 6" lead wall downscatters the high energy neutrons by a significant amount, with the result that the E*ϕ(E) "spectrum" for the 6" Pb penetration peaks at about 0.8 MeV, whereas the corresponding source "spectrum" (Figure 12) peaks at about 3 MeV. This is due to the energy dependence of the neutron inelastic scattering cross section for lead; it is roughly equal to 50% of the total cross section at 6 MeV and above, and drops by over an order of magnitude from 6 MeV to 1 MeV, where it becomes essentially negligible. Thus, the neutrons below 1 MeV are "built up" by down-scattering from higher energies. The result is a shifting of the peak of the E*ϕ(E) "spectrum" from about 3 MeV down to about 0.8 MeV. (See Figures 11 and 14 above.) If one normalizes the two spectra in the 0.1 to 0.8 MeV region, the two will be seen to differ by a factor of 3 to 4 in the few MeV region. In previous work done by the authors[2], this degree of spectrum "softening" was obtained with only 2" of iron shielding: The inelastic scattering cross section for iron is quite large down to about 0.8 MeV. Thus, with a medium to high atomic weight shield, the neutron spectrum becomes appreciably softened.

It is interesting to note that the spectral difference between the free field and 6" Pb wall + cave cases is great enough wherein the thought of useful spectral-dependence experiments might be entertained for comparing "equidose" exposures for the two cases of widely differing neutron spectra. Such experiments would probably have to be confined to those where the gamma-ray sensitivity is low because it is much different relative to the two neutron dosages. An example of this is the measurement of transistor damage in different neutron spectra.

With a water shield, the effect is a hardening of the neutron spectrum. This arises from a rapid overall decrease in neutron cross section with increasing energy for both hydrogen and oxygen above 1 MeV: The higher energy neutrons become quite transparent. A comparison of the free-field spectrum, Figure 16, with the spectrum calculated for the reactor moved back 12" into the water (Figure 17) shows a dramatic difference. The peak energy for the 12" water shield is moved up to the 4-8 MeV region. Also, the E*ϕ(E) "spectrum" drops by about two orders of magnitude below the peak value for energies below 0.1 MeV where the 1/E spectral dependence finally sets in.

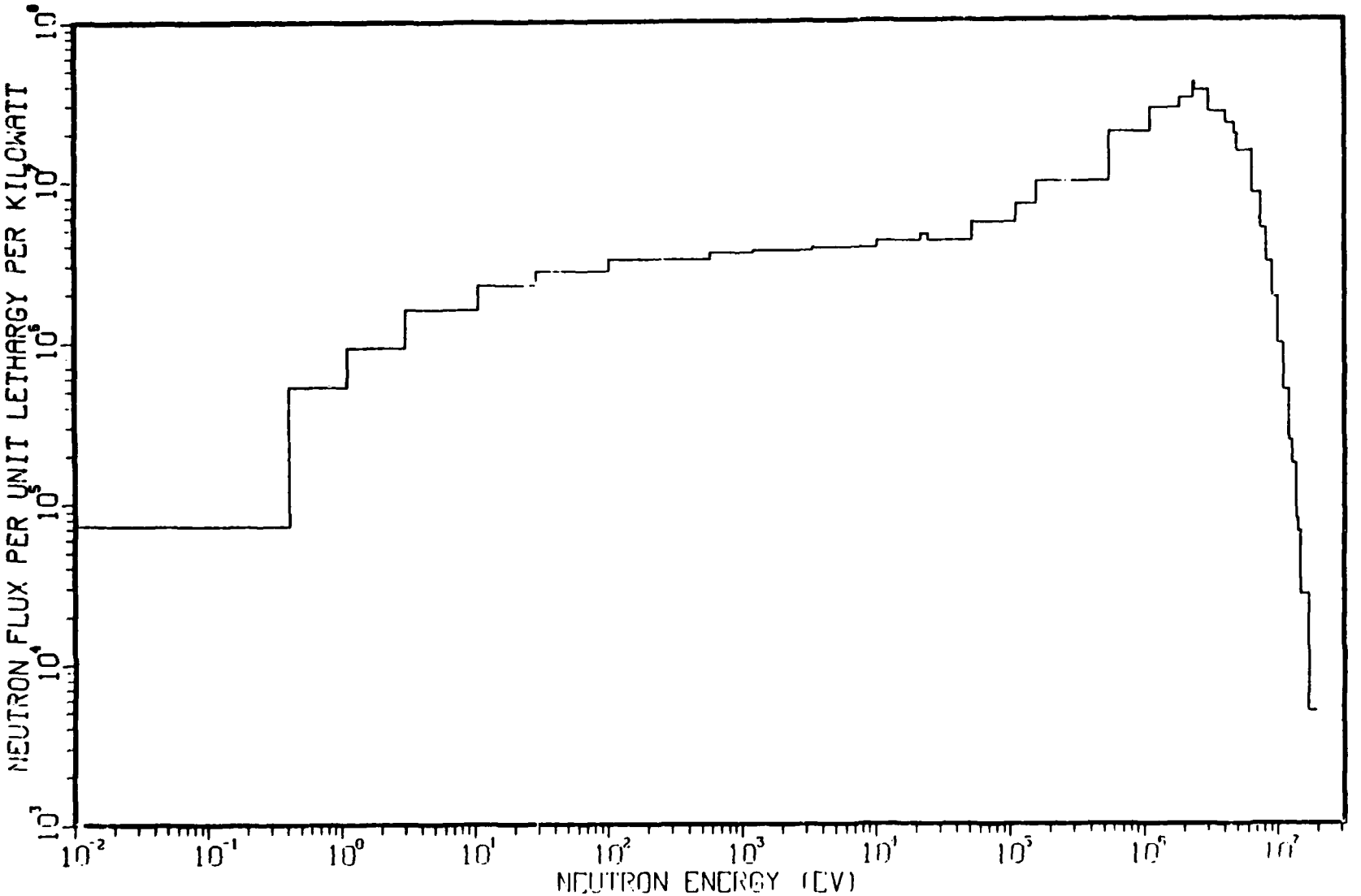

Figure 16. Total (Front+Back, 1-D) Neutron Flux vs Energy ER1 Free Field.

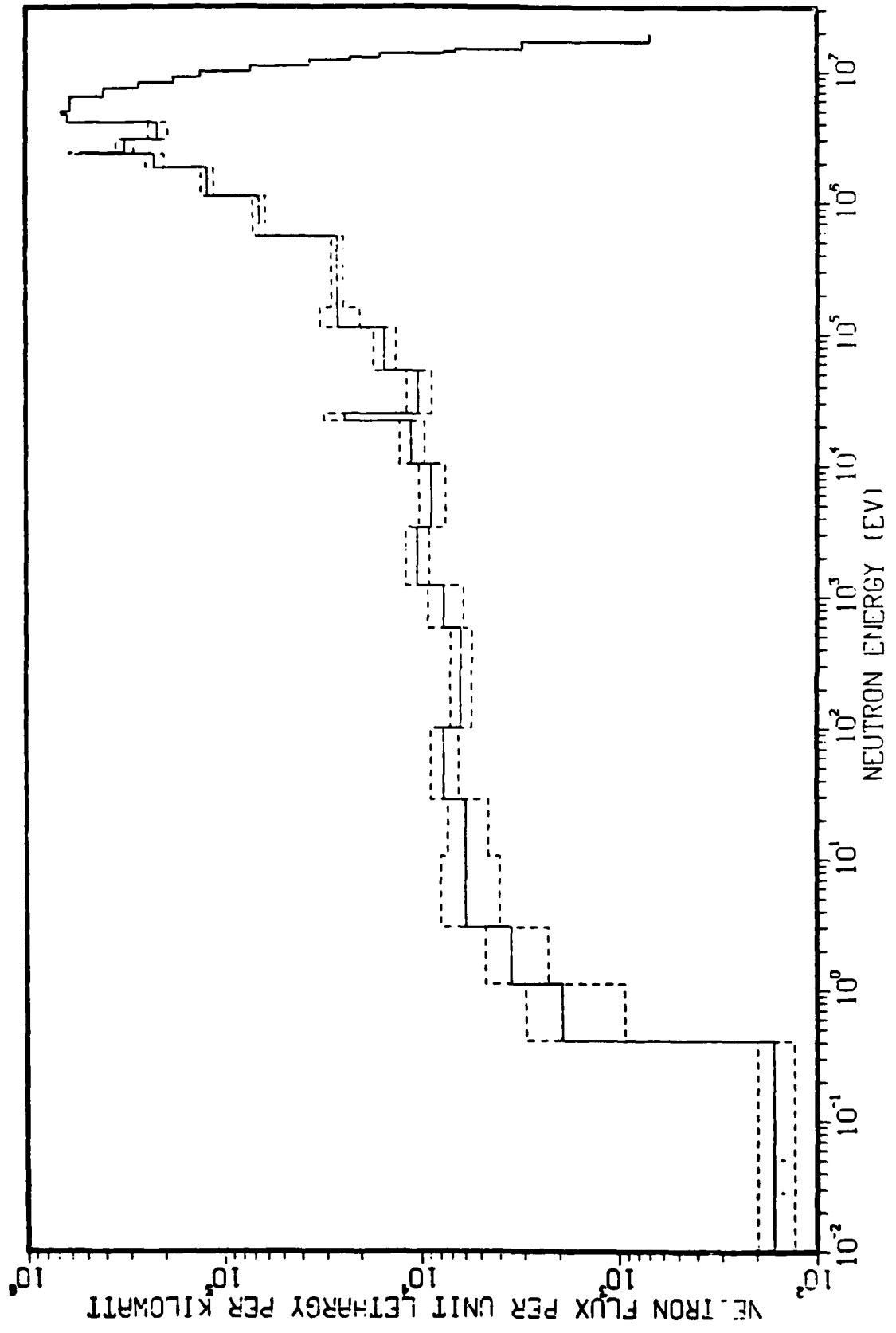

Figure 17. Total (Front+Back) Neutron Flux vs Energy ERI Free Field with 12" Water.

The above methods of obtaining very diverse spectra were used for experiments with transistors[2], wherein the measured damage was compared to that calculated for exposure to widely varying neutron spectra. The validity of the calculated silicon damage function $D(E_n)$ was verified, since the measured damage and that calculated from $\int D(E_n)\phi(E_n)dE_n$ agreed for exposures to widely differing spectra. With the use of only 2" of iron to obtain a softened fast-neutron spectrum, and 4" of polyethylene for a hardened one, the two differed by about a factor of 10 above several MeV, when normalized at the 0.2 MeV threshold energy for damage to silicon semiconductor material.

In this way, a TRIGA reactor such as the AFRRI reactor can be used to study the energy dependence of other semiconductor materials such as GaAs or Ge, of electrical insulators materials, of structural materials such as steel, and other radiation effects which do not have a strong gamma-ray irradiation dependence.

5. CHARACTERIZATION OF THE NEUTRON FIELDS FOR SILICON DAMAGE EFFECTIVENESS

The silicon-damage characterization for each of the five measurements is presented in Table 5. These values are for total fluence and not flux/kW. Note in Table 1 that the free field measurements (Runs 2 and 4) were carried out for a total of 150 MW-sec, the 6" lead wall + 2" cave case (Run 1) for 450 MW-sec, the exercise wheel (2" Pb) for 225 WM-sec, and the phantom behind 6" Pb for 600 MW-sec.

Normalizing to a standard factor power * time, one finds that the 1 MeV equivalent flux (ϕ_{eq}, Column 5) is 28% higher for the free field case than for the 6" Pb wall shield and 2" cave. Yet, the flux above 10 keV is the same for both. Thus, the softer neutrons emerging from the 6" lead wall have 28% less effect on silicon. The higher energy neutrons are more damaging, as can be seen by the $D(E_n)$ curve for silicon given in References 2 and 5.

The "spectral shape factor" ϕ_{eq}/ϕ given in Column 7 shows the damageability per neutron above 10 keV. These values also differ by nearly 28%, in agreement with the conclusions of the preceding paragraph.

Note that the difference in ϕ_{eq}/ϕ for exercise wheel behind 2" Pb wall versus ER-1 and ER-2 free field is about 1/3 that for 6" Pb + cave versus free field, as might be expected.

Adding tissue-shielding (~3½" radius) to the 6" Pb shield (Run 5) results in only a very slight hardening of the spectrum: ϕ_{eq}/ϕ increases by only 2%. However, the effect of the tissue on the total neutron flux is nothing short of dramatic. While the 6" Pb shield and cave had no effect on total neutron flux, the addition of the 3½" radius phantom reduced the flux by a factor of 4! This arises from the softening of the neutron spectrum by lead, combined by the large increase in hydrogen cross section between the 3 MeV peak in $E*\phi(E)$ for free-field neutrons and the 0.8 MeV peak for neutrons through the 6" Pb shield. The free field high-energy neutrons are attenuated by about 1%/mm in water, or a factor of 2.6 for 3½" of water (tissue). This is to be compared to the factor of 4 for lead-moderated neutrons in 3½" of water.

Table 5. Spectral Parameters for AFRRI TRIGA. $D(E_n)$ is the total neutron "damage" (energy deposit) in Rads Silicon.

Run #	Configuration	$\int_{.01}^{18.0} \phi DdE$	$\overline{D}$ (1 MeV)	ϕ_{eq}†	ϕ†>.01 MeV	ϕ_{eq}/ϕ	$N_{ni}\lambda$†	$\phi/N_{ni}\lambda$	$\phi_{eq}/N_{ni}\lambda$
1	ER1-6" Pb	6.11+2*	2.04-11	3.00+13	3.14+13	0.955	8.93-20	3.52+32	3.36+32
2	ER2-FREE FLD.	2.62+2	2.04-11	1.28+13	1.05+13	1.22	1.07-19	9.81+31	1.20+32
3	ER1-2" Pb/EX WHL	3.73+2	2.04-11	1.83+13	1.64+13	1.12	1.03-19	1.59+32	1.78+32
4	ER1-FREE FLD	2.54+2	2.04-11	1.25+13	1.02+13	1.23	1.05-19	9.71+31	1.19+32
5	ER1-6" Pb/PHANTOM	2.03+2	2.04-11	9.95+12	1.02+13	0.976	4.39-20	2.32+32	2.27+32

* Read as 6.1×10^2

† ϕ_{eq}, $\phi \geq .01$ MeV, and N_{ni} are determined from the foils in the boron ball. These numbers must be multiplied by 1.13 to obtain the fluence/activations outside the ball.

Note that the measured total neutron flux above 10 keV, Table 4, and the ϕ_{eq}, Table 5, are nearly identical for ER-1 and ER-2 free field runs (Run 2 and Run 5, respectively). Yet the calculated values (Table 4) differ by 25%. This is further established by the independent nickel-foil threshold neutron detector results shown in Column 8 of Table 5. This further underlines the necessity for normalizing all calculational results to the measured data for the measured configuration that is nearest to that being calculated.

The nickel-foil monitor has proven to be much more reliable than the sulfur monitor. For this reason, the nickel-foil activation data is presented in Columns 8, 9 and 10 in Table 5. Column 8 presents the foil activation, Column 9 the neutrons above 10 keV per activation/nucleus, and Column 10 the 1-MeV equivalent fast-neutron fluence per activation/nucleus.

The nickel foil is activated only by neutrons above about 3 MeV. It is interesting to compare the nickel foil activations for the ER-1 free-field case and 6" Pb shield and cave case, where the neutron flux above 10 keV is the same. The nickel foil activations, on a per-kilowatt basis, are a factor of 4 greater for the free-field case, which illustrates how much harder this spectrum is. The biological dose and transistor damage for fast neutrons are much greater in the free-field case, where the massive slowing down of neutrons has not occurred.

One can semi-quantitatively obtain neutron-spectrum "hardness" data of this nature from as few as two foils. The U-235 data of Table 2 show nearly the same activation level per kilowatt for Runs 1 and 2 (6" Pb + cave versus free field). This agrees with the integral flux above 10 keV, and it shows almost no variation above 10 keV whereas the nickel foil shows a factor of 4 difference above 3 MeV. A nickel/U-238 "spectrometer" such as this is about the simplest imaginable, conceptually. Yet, it produces sensitive radiation-hardness data for both electronics damage, and biological damage, and possibly for damage to structural materials and electrical insulators as well.

6.0 SUMMARY AND CONCLUSIONS

The radiation fields for the AFRRI reactor have been measured with good accuracy for all energies of interest, and for five widely different geometries commonly used at that facility. The silicon damage can be determined from these data with an estimated precision of 1-3%. The accuracy has perhaps an order of magnitude smaller uncertainty than achievable in the 1960's, when the last determination was made. This for the most part is due to increased accuracy in cross sections, to better known nuclear data in other respects (fission yields, gamma fluorescent yields), better calculational accuracy, the use of the calculated spectral shape in unfolding of the measured neutron spectrum, the availability of large computers and a neutron-spectrum unfolding code that requires these machines, and the availability of much better gamma-ray detectors and accurately calibrated (NBS) gamma-ray line sources.

The calculated data, when normalized to the measured data of nearly the same configuration, can be of great value for accurate estimates of neutron fields. In this way, accurate planning future experiments will be greatly facilitated if these data are fully utilized.

REFERENCES

1. C. Cassapakis and V.V. Verbinski, "Neutron Radiation Damage Characterization Versus Distance from Berkeley Reactor," SAI Report No. SAI-272-80-371-LJ, San Diego, California, May 22, 1980.

2. V.V. Verbinski, C. Cassapakis, R. L. Pease and H.L. Scott, "Transistor Damage Characterization by Neutron Displacement Cross Section in Silicon: Experimental," Nucl. Science and Engineering 70, 66 (1979).

3. J.A. Sayeg, "Neutron and Gamma Dosimetry Measurements at the AFRRI-DASA TRIGA Reactor," AFRRI CR65-6, Armed Forces Radiobioloby Research Institute, November, 1965.

4. ASTM Standards: (a) E-720-80 Standard Guide for Selection of a Set of Neutron Activation Foils for Determining Neutron Spectra Used in Radiation Hardness Testing of Electronics. (b) E-721-80 Standard Method for Determining Neutron Spectra with Neutron Activation Foils for Radiation Hardness Testing of Electronics. (c) E-722-80, Standard Practice for Characterizing Neutron Energy Fluence Spectra in Terms of an Equivalent Monoenergetic Neutron Fluence for Radiation Hardness Testing of Electronics.

5. V.V. Verbinski, C. Cassapakis, R.L. Pease and H.L. Scott, "Simultaneous Neutron Spectrum and Transistor-Damage Measurements in Diverse Neutron Fields: Validity of $D_{S_i}(E_n)$." LRL Memorandum Report 3929, March 16, 1979, Naval Research Laboratory, Washington, D.C.

6. W.N. McElroy, et al, AFWL-TR-67-41, Vol. 1, Air Force Weapons Lab, (1967).

DISTRIBUTION LIST

DEPARTMENT OF DEFENSE

U.S. Documents Officer
AFSOUTH
ATTN: U.S. Documents Ofc for Col Hunter

Armed Forces Radiobiology Rsch Institute
Defense Nuclear Agency
National Naval Medical Center
ATTN: Director
ATTN: Deputy Director
ATTN: HEAD, SAF
ATTN: HEAD, RSD
ATTN: HEAD, CSD
ATTN: Chief, RSRP
ATTN: Chief, RSRS
ATTN: CPT, ALT
ATTN: LT Blake
ATTN: Mr. Webber
ATTN: LTC Conklin
ATTN: CDR Devine
ATTN: Dr. Hsieh
ATTN: Dr. Ledney
ATTN: Mr. Moore
ATTN: CPT Sholtis
ATTN: MAJ Smoker
3 cy ATTN: Library
10 cy ATTN: CPT Bice
14 cy ATTN: LT K. Ferlic

Assistant Secretary of Defense
Program Analysis & Evaluation
ATTN: S. Sienkiewiez
ATTN: Strategic Programs

Assistant to the Secretary of Defense
Atomic Energy
ATTN: L. Michael
ATTN: Strategy & Assessment
ATTN: Executive Assistant
ATTN: T. Sisson
ATTN: Nuclear Policy Planning

Defense Intelligence Agency
ATTN: DR-4C, J. Burfening
ATTN: DB 4C, E. O'Farrell
ATTN: DN
ATTN: RTS-2C
ATTN: Library
ATTN: DIO-GPF, W. Magathan
ATTN: DT, J. Vorona
ATTN: DB-4C, P. Johnson

Defense Technical Information Center
12 cy ATTN: DD

Field Command
Defense Nuclear Agency
ATTN: FCLS, D. Norton
ATTN: FCLS
ATTN: FCPR, J. McDaniel

Field Command
Defense Nuclear Agency
Livermore Branch
ATTN: FCPRL

DEPARTMENT OF DEFENSE (Continued)

Field Command
Defense Nuclear Agency
Los Alamos Branch
ATTN: FCPRA

Interservice Nuclear Weapons School
ATTN: TTV
ATTN: *Document Control*

Joint Chiefs of Staff
ATTN: J-5 Nuclear Division/Strategy Div

Under Secretary of Defense for Rsch & Engrg
ATTN: *M. Minneman*
ATTN: F. McLeskey
ATTN: Strategic & Space Sys (OS)
ATTN: *K. Hinman*

Defense Nuclear Agency
ATTN: NASD
ATTN: NAFD
ATTN: GC
ATTN: PAO
ATTN: NATD
ATTN: SPTD
ATTN: RAAE
ATTN: NATA
ATTN: STNA
ATTN: STRA
ATTN: STSP
4 cy ATTN: TITL
5 cy ATTN: NTPR
10 cy ATTN: BA
10 cy ATTN: NATD/D AUTON

DEPARTMENT OF THE ARMY

Army Library
Department of the Army
ATTN: Military Documents Section

Deputy Chief of Staff for Rsch Dev & Acq
Department of the Army
ATTN: DAMA-CSM-N

Harry Diamond Laboratories
Department of the Army
ATTN: Chief Div 30000
ATTN: 00100 Commander/Tech Dir/TSO
ATTN: DELHD-N-D
ATTN: DELHD-N-RBG
ATTN: DELHD-N-TD
ATTN: DELHD-N-P
ATTN: Chairman, Nuc Vulnerability Branch

U.S. Army Armament Rsch Dev & Cmd
ATTN: DRDAR-LCN-E

U.S. Army Ballistics Research Lab
ATTN: DRDAR-BLB
ATTN: DRDAR-VL
ATTN: DRDAR-TBS-S
ATTN: DRDAR-BLV

DEPARTMENT OF THE ARMY (Continued)

U.S. Army Center of Military History
ATTN: DAMH

U.S. Army Chemical School
ATTN: ATZN-CM-CS
ATTN: ATZN-CM-AL

U.S. Army Fa Msl Sys Eval Gp
ATTN: ATZR-MG

U.S. Army Foreign Science & Tech Ctr
ATTN: DRXST-SD-I

U.S. Army Material Sys Analysis Actvy
ATTN: X5 (W3JCAA)

U.S. Army Mobility Equip R&D Cmd
ATTN: DRDME-RT, K. Oscar
ATTN: DRDME-WC Technical Library (Vault)

U.S. Army Nuclear Chemical Agency
ATTN: Library
ATTN: MONA-ZB, D. Panzer

U.S. Army TRADOC Sys Analysis Actvy
ATTN: ATAA-TAC

10th Med Lab
Department of the Army
4 cy ATTN: CPT E. Daxon

DEPARTMENT OF THE NAVY

Aviation History Unit
Office of the Deputy CNO
Department of the Navy
ATTN: Library

Bureau of Medicine and Surgery
Department of the Navy
ATTN: Assistant for Medical Surgery

Joint Cruise Missiles Project Ofc
Department of the Navy
ATTN: JCMG-707

Merchant Marine Academy
Department of the Navy
ATTN: Director of Libraries

Naval Postgraduate School
ATTN: Code 56PR
ATTN: Code 1424, Library
ATTN: Code 61, J. Dyer

Naval Research Laboratory
ATTN: Code 2627
ATTN: Library

Naval School of Health Sciences
ATTN: Library

Naval Sea Systems Command
ATTN: SEA-406
ATTN: Nuclear Technology Div
ATTN: SEA-06H2
2 cy ATTN: SEA-6431G, H. Seguine

DEPARTMENT OF THE NAVY (Continued)

Naval Surface Weapons Center
ATTN: Code F30
ATTN: Code U41
ATTN: Code R14
ATTN: Code F31
ATTN: Code U12
ATTN: Code R41, H. Scofield

Naval Surface Weapons Center
ATTN: Code DG-502, E. Freiling
ATTN: Library

National Medical Center
Department of the Navy
ATTN: RAD Safety, C-45, LCDR Zeman

Naval Weapons Center
ATTN: Code 32607, L. Thompson
ATTN: Code 233

Naval Weapons Evaluation Facility
ATTN: G. Binns
ATTN: Technical Director
ATTN: J. Abbott
ATTN: Library

Navy Dept Library
ATTN: Library

Navy Nuclear Power School
Naval Training Center
ATTN: Library

Nimitz Library
U.S. Naval Academy
ATTN: Documents & Reports Dept

Office of Naval Research
ATTN: Code 431
ATTN: Code 200

Surface Warfare Development Group
Naval Amphibious Base
ATTN: Commander

U.S. Merchant Marine Academy
Academy Library
Department of the Navy
ATTN: Library

DEPARTMENT OF THE AIR FORCE

Academy Library Dfseld
U.S. Air Force Academy
ATTN: Library

Aerospace Defense Command
Department of the Air Force
ATTN: Historian

Air Force Institute of Technology
Air University
ATTN: ENP
ATTN: Library

Air Force Technical Applications Ctr
ATTN: Historian

DEPARTMENT OF THE AIR FORCE (Continued)

Air Force Test & Evaluation Center
ATTN: OA

Air Force Weapons Laboratory
Air Force Systems Command
ATTN: SUL
ATTN: Tech Library
ATTN: NSSB
ATTN: NT
ATTN: NXS

Air University Library
Department of the Air Force
ATTN: AUL-LSE

Ballistic Missile Office
Air Force Systems Command
ATTN: ENSN
ATTN: SYE

Deputy Chief of Staff
Research, Development & Acq
Department of the Air Force
ATTN: AFRDQR
ATTN: AFRDQI

U.S. Air Force Occupational & Env Health Lab
ATTN: NTPR

USAF School of Aerospace Medicine
ATTN: Radiation Sciences Div
ATTN: Strughold Library
ATTN: RZW, Maj Cordts

DEPARTMENT OF ENERGY

Department of Energy
ATTN: OMA

Department of Energy
Division of Reactor Rsch and Dev
ATTN: P. Hemmig

OTHER GOVERNMENT AGENCIES

Centers for Disease Control
ATTN: G. Caldwell

Central Intelligence Agency
ATTN: Office of Medical Services
ATTN: OSWR/NED
ATTN: OSR/SE/F

Department of Commerce
National Bureau of Standards
Center for Radiation Research
ATTN: J. Hubell
ATTN: Library

Department of Health & Human Svcs
ATTN: Office of General Counsel

Library of Congress
ATTN: Serial & Govt Publication
ATTN: Science & Technology Div
ATTN: Library Service Division

OTHER GOVERNMENT AGENCIES (Continued)

National Technical Information Service
ATTN: Customer Service

U.S. Coast Guard Academy
Department of Transportation
ATTN: Library

U.S. Military Academy
ATTN: Director of Libraries

OTHER

Brookhaven National Laboratory
ATTN: Nat Neu Cross Sec, S. Pearlstein

DEPARTMENT OF ENERGY CONTRACTORS

Lawrence Livermore National Lab
ATTN: Technical Info Dept Library
ATTN: L-71, R. Howerton
ATTN: L-35, J. Immele
ATTN: L-531, A. O'Dell
ATTN: L-9, R. Barker
ATTN: L-21, M. Gustavson
ATTN: L-8, F. Barrish

Los Alamos National Laboratory
ATTN: F. Begay
ATTN: R. Sandoval
ATTN: M/S 634, T. Dowler
ATTN: D. Harris
ATTN: Library
ATTN: E. Chapin
ATTN: R. Stolpe
ATTN: ADPA MMS 195

Oak Ridge National Laboratory
Nuclear Division
ATTN: C. Clifford
ATTN: Central Rsch Library
ATTN: Rad Shielding Ctr
ATTN: F. Mynatt

Reynolds Electrical and Engr Co, Inc
ATTN: CIC
ATTN: W. Brady

Sandia National Laboratories
Livermore National Laboratory
ATTN: T. Gold
ATTN: Library & Security Classification Div

Sandia National Laboratory
ATTN: Central Library
ATTN: W. Hereford
ATTN: 5612, J. Keizur
ATTN: 3141

DEPARTMENT OF DEFENSE CONTRACTORS

Analytical Technology Applications Corp
ATTN: J. Scharfen

Atmospheric Science Assoc
ATTN: H. Normeat

DEPARTMENT OF DEFENSE CONTRACTORS (Continued)

BDM Corp
ATTN: J. Bode
ATTN: R. Welander
ATTN: P. White
ATTN: J. Herzog
ATTN: H. Portnoy
ATTN: R. Buchanan
ATTN: J. Braddock
ATTN: J. Morgan
ATTN: C. Somers
ATTN: C. Wasaff

Boeing Co
ATTN: A. Lowrey
ATTN: L. Harding

Decision-Science Applications, Inc
ATTN: Dr. Pugh

Garjak Research, Inc
ATTN: G. Jacobson

General Research Corp
ATTN: A. Berry
ATTN: P. Lowry
ATTN: Tactical Warfare Operations
ATTN: H. Schroeder

Hudson Institute, Inc
ATTN: H. Kahn
ATTN: C. Gray

Institute for Defense Analyses
ATTN: M. Schafer
ATTN: Classified Library

IRT Corp
ATTN: Library

JAYCOR
ATTN: A. Nelson
ATTN: E. Almquist
10 cy ATTN: Health & Environment Div

Kaman Sciences Corp
ATTN: V. Cox
ATTN: F. Shelton

Kaman Sciences Corp
ATTN: T. Long

Kaman Tempo
ATTN: DASIAC
ATTN: E. Martin

Kaman Tempo
ATTN: R. Miller

Kaman Tempo
ATTN: C. Jones

Lockheed Missile & Space Co, Inc
ATTN: TIC-Library

Martin Marietta Corp
ATTN: M. Yeager
ATTN: F. Marion

DEPARTMENT OF DEFENSE CONTRACTORS (Continued)

McDonnell Douglas Corp
ATTN: Technical Library Services

McLean Research Center, Inc
ATTN: W. Schilling

Mission Research Corp
ATTN: Tech Library

National Academy of Sciences
ATTN. C. Robinette
ATTN: National Materials Advisory Board
ATTN: Medical Follow-up Agency

Manteon International Corporation
ATTN: President

Pacific-Sierra Research Corp
ATTN: G. Lang
ATTN: H. Brode

Pacific-Sierra Research Corp
ATTN: G. Moe
ATTN: D. Gormley

R & D Associates
ATTN: J. Lewis
ATTN: P. Haas
ATTN: F. Field
ATTN: R. Montgomery
ATTN: A. Lynn

R & D Associates
ATTN: J. Bengston
ATTN: J. Thompson
ATTN: W. Houser

Radiation Research Associates, Inc
ATTN: Library

Rand Corp
ATTN: T. Parker
ATTN: J. Digby
ATTN: Library

Raytheon Co
ATTN: W. Britton

University of Rochester
ATTN: NAVWAG

Santa Fe Corp
ATTN: D. Paolucci

Science Applications, Inc
ATTN: J. Martin
ATTN: M. Drake
ATTN: E. Straker
ATTN: W. Woolson
ATTN: C. Whittenbury
4 cy ATTN: W. Hagan
4 cy ATTN: V. Verbinski
4 cy ATTN: C. Cassapakis

Science Applications, Inc
ATTN: N. Byrn
ATTN: T. Albert

DEPARTMENT OF DEFENSE CONTRACTORS (Continued)

Science Applications, Inc
ATTN: W. Layson
ATTN: J. McGahan
ATTN: Tech Library
ATTN: J. Goldstein

Science Applications, Inc
ATTN: D. Kaul

Science Applications, Inc
10 cy ATTN: L. Novotney

SRI International
ATTN: W. Jaye
ATTN: G. Abrahamson
ATTN: J. Naar
ATTN: P. Dolan

System Planning & Analysis, Inc
ATTN: P. Lantz

Advanced Research & Applications Corp
ATTN: H. Lee

DEPARTMENT OF DEFENSE CONTRACTORS (Continued)

System Planning Corp
ATTN: G. Parks
ATTN: J. Douglas
ATTN: F. Adelman

S-CUBED
ATTN: Library

T. N. Dupuy Associates, Inc
ATTN: T. Dupuy

Tetra Tech, Inc
ATTN: F. Botnwell

TRW Electronic & Defense Sector
ATTN: R. Anspach

Vector Research, Inc
ATTN: S. Bonder

Aerospace Corp
ATTN: Library